Density functional theory study of Fe, Co, and Ni adatoms and dimers adsorbed on graphene

Harman Johll and Hway Chuan Kang*
Department of Chemistry, National University of Singapore, Singapore 119260, Singapore

Eng Soon Tok
Department of Physics, National University of Singapore, Singapore 119260, Singapore
(Received 19 September 2008; revised manuscript received 27 April 2009; published 12 June 2009)

Metal clusters have been investigated rather intensely for both fundamental and technological reasons. In this work we report the results of plane-wave density functional theory calculations of Fe, Co, and Ni adatoms and dimers adsorbed on graphene. We study both homonuclear and heteronuclear dimers, and the latter includes mixed dimers of Fe, Co, and Ni along with dimers of these elements with Pt. Our work is motivated by the fundamental interest in their configurational and magnetic properties. We calculated the adsorption site, the structure and relative stabilities of various adsorption configurations, the band structures, the atomic projected electronic density of states, and the magnetic moments of the adatoms and dimers. Contrary to previous work, our results show that adatoms bind weakly to graphene with binding energies ranging from 0.2 to 1.4 eV depending on the adsorption site and species. For both homonuclear and heteronuclear dimers the binding energies per atom are lower than the respective adatom cases, ranging from 0.1 to 0.5 eV per metal atom. The most strongly bound configurations for all the dimers studied are those with the dimer axis (nearly) perpendicular to the graphene plane and bound at the hole site. These configurations, which, to our knowledge, have not been considered in previous work, also turn out to have the largest enhancement of the magnetic moment at least for the atom farther from the graphene. The binding energies of these most strongly bound dimers are dependent on three factors, namely, the interconfigurational energy change in the dimer atom farther from graphene upon desorption, the charge transfer from the dimer to the graphene, and the adsorption site favored by the atom closer to the graphene sheet. The first factor is dominant for all the dimers studied here except for CoPt and NiPt. The relatively high electronegativity of Pt affects the character of the charge transfer from the dimer to graphene. In most of the dimers we investigated, charge is transferred almost exclusively from the dimer atom closer to the graphene except for heteronuclear dimers with Pt where charge is also transferred between the two dimer atoms upon adsorption. Thus, our calculations of the electronic structure allow us to understand the trends in binding energy and the magnetic moment in these dimers.

DOI: 10.1103/PhysRevB.79.245416 PACS number(s): 68.43.−h

I. INTRODUCTION

Research interest in transition metal clusters continues to grow given their wide range of applications from catalysis to nanomagnetic devices. In particular, clusters of the ferromagnetic elements, Fe, Co, and Ni, have been shown to be important in heterogeneous catalysis and are known to display magnetic moments that are very much enhanced relative to their bulk magnetic moments ($2.2\mu_B$/atom, $1.7\mu_B$/atom, and $0.7\mu_B$/atom, respectively). Small homonuclear clusters of the ferromagnetic metals Fe, Co, and Ni have been shown to exhibit high magnetic moments that increase nonmonotonically (or in an oscillatory manner) with decreasing cluster size (for example, see Ref. 1), with sharp peaks occurring at certain "magic" cluster size. The high surface-to-volume ratio of these clusters results in fewer bonds per metal atom and therefore frees up nonbonded valence electrons which if left unpaired gives rise to an enhanced magnetic moment. The magnetic moments of these clusters are therefore extremely sensitive to the cluster geometry[2–5] and the environment in which the cluster is placed in.[6–12]

Small homonuclear clusters of the ferromagnetic metals Fe, Co, and Ni have been shown to exhibit high magnetic moments that increase nonmonotonically (or in an oscillatory manner) with decreasing cluster size (for example, see Ref. 1), with sharp peaks occurring at certain magic cluster size. The high surface-to-volume ratio of these clusters results in fewer bonds per metal atom and therefore frees up nonbonded valence electrons which if left unpaired gives rise to an enhanced magnetic moment. Furthermore, combinations of transition metals are also of interest in this respect. Simple alloying of the transition metals, which can result in bulk phases with enhanced magnetic moments relative to the bulk phase of the respective components depending on the composition used, does not suffice for current technological demands. The maximum of the Slater-Pauling curve, which is a plot of the average magnetic moment per atom in a bulk phase system, occurs for a $Fe_{0.7}Co_{0.3}$ bulk phase system at a value of $2.45\mu_B$. Nanoscale magnetic materials offer the possibility of going beyond this Slater-Pauling maximum. Some examples of such materials that have been investigated include CoPt nanoparticles,[13–15] Fe clusters embedded in Co,[8–10] FePt nanoparticles,[16] and the small homonuclear[1–12,17–21] and heteronuclear transition metal clusters. Like the bulk phase binary alloys of the transition metal elements, binary transition metal clusters have been shown to exhibit projected magnetic moments that are higher or lower than the magnetic moments of the corresponding free metal atoms depending on the composition of the heteronuclear cluster. Andriotis *et al.*[22] found that the redistribution of electrons in the molecular orbitals of these clusters could give rise to projected magnetic moments that are

greater than the corresponding free-atom values but may result in total cluster moments that are reduced depending on whether the projected spins align ferromagnetically or antiferromagnetically with one another. For example, they found that the Co atom in CoX_n (where X=Fe, Co, or Ni and n=1 or 2) clusters has a magnetic moment that is ferromagnetically aligned with respect to μ_X which thus implies an overall enhancement of the total magnetic moment of the cluster. The magnetic moment on the Co atom in such clusters is not affected by the choice of X. Though smaller than the magnetic moment of the free Co atom, it is still larger than the bulk value of $1.7\mu_B$. Fe in FeX_n clusters on the other hand does not display any systematic trend in that its spin may align either ferromagnetically or antiferromagnetically with the spin of its neighboring atom(s) thus giving rise to magnetic moments that are either enhanced or reduced relative to the sum of the absolute values of the calculated atomic magnetic moments of the cluster-constituent atoms. Xie and Blackman[8] showed that the Fe clusters over a size range of 100–600 atoms embedded in a Co matrix have magnetic moments that are comparable to that of the free clusters. However, when embedded in a matrix of Cu atoms, these Fe clusters had magnetic moments that are lower compared to that of free clusters though still higher than the Fe bulk limit of $2.2\mu_B$. Studying the same system of Fe clusters embedded in a Co matrix, Bergman *et al.*[9] found that clustering lowers the average magnetic moment compared to ordered structures and random alloys.

In a thorough theoretical study of the 3*d* transition metal dimers, Gutsev *et al.* calculated the projected magnetic moments (among a host of other physical properties such as the dipole moments, bond dissociation energies, and ionization energies to name a few) for both the homonuclear and heteronuclear dimers. For the FeCo and FeNi dimers, they found that the Fe atom has its magnetic moment enhanced compared to the Fe atom in an FeFe dimer ($3.2\mu_B$ and $3.4\mu_B$ for Fe in FeCo and FeNi, respectively, compared to $3.0\mu_B$ for Fe in FeFe). The Co and Ni atoms on the other hand had their spin reduced compared to the projected moments of the Co and Ni atoms in the CoCo and NiNi dimers ($1.8\mu_B$ for Co in FeCo compared to $2.0\mu_B$ in CoCo and $0.6\mu_B$ for Ni in FeNi compared to $1.0\mu_B$ in NiNi). In the case of the CoNi dimer, the Co atom has an enhanced magnetic moment ($2.2\mu_B$) while the Ni atom has a reduced magnetic moment ($0.8\mu_B$). The sum of the projected magnetic moments of the FeCo, FeNi, and CoNi dimers is in fact the same as the sum of the projected magnetic moments of these atoms when in their homonuclear free dimer state. The enhancement in magnetic moment in order of Fe>Co>Ni is consistent with the relative electronegativity of these species. Being the most electronegative among the three, Ni tends to draw in electron density which then gives results in the pairing of spin thus lowering its projected magnetic moment compared to the Ni atom in the NiNi dimer. Fe on the other, being the least electronegative, would have its magnetic moment enhanced compared to the Fe atom in the FeFe dimer. This delicate interplay of *d*-orbital filling proves the key in enhancing the magnetic moments of these binary clusters.

The resulting unique physical and chemical properties are therefore dependent on whether they are bound to a surface and then on the nature of that surface. Thus, much research has gone into investigating the effects that various support materials have on the physical and chemical properties of these metal clusters when bound to them: silver,[12] platinum,[11] palladium,[11] and the family of carbon allotropes, namely, graphite,[7,23–26] graphene,[6,7,17,23] carbon nanotubes,[6,20] and fullerene.[26,27] Ideally one looks for a support material that does not alter the physical and chemical properties of the bound cluster by too much compared to when the cluster is free, viz., one that is sufficiently inert in terms of its reactivity with the transition metal clusters but at the same time allows for the clusters to bind sufficiently well to it. While metal surfaces interact rather strongly with metal clusters, graphite is known to be reasonably inert. The recent isolation of graphene[28] has sparked off intense research interest in uncovering its novel properties.[29–33] Coupling graphene with other materials might also allow for an integration of novel technologies (e.g., superconductivity and spintronics). We are therefore motivated to study, at least as a starting point, the physical properties of the Fe, Co, and Ni adatoms and dimers on graphene.

Due to their size, our fundamental understanding of small metal clusters is still lacking. Experiments are not able to accurately probe certain physical properties of these small metal clusters (e.g., the electronic structure) given the extremely small physical quantities that need to be measured in order to determine such properties (e.g., the atomization energies). The difficulties associated with treating the complex 3*d*-4*s* exchange interactions associated with transition metal atoms limit theoretical calculations of these clusters although considerable effort has been taken over the last 20 years to improve the quality and level of theory specific to modeling transition metal atoms and its clusters.

In the context of transition metal clusters bound on graphene, particularly those of the ferromagnetic elements, little experimental work[24,25,34] has been done thus far. Theoretical calculations[6,7,17] have been done using many different methods to estimate the binding energies and the magnetic moments among other things. For example, the binding energies obtained from the density functional theory (DFT) (Vosko-Wilk-Nusair[35] for the exchange-correlation functional and using a linear combination of atomic orbitals as the basis set) cluster calculations of Duffy and Blackman[7] suggest that the adatoms and to some extent the dimers are chemisorbed on graphene (e.g., 2.0, 2.4, and 2.5 eV for Fe, Co, and Ni adatoms, respectively, above the middle of a hexagon, i.e., a hole site) although there is only a small charge transfer to the graphene. The spin-polarized first-principles pseudopotential (ultrasoft) plane-wave DFT [PW91 (Ref. 36) for the exchange-correlation functional] calculations of Yagi *et al.*[6] (using a kinetic energy cutoff of 287 eV) suggest adatom chemisorption as well but with values that are on average 1 eV lower than those suggested by Duffy and Blackman. The linear muffin-tin orbital calculations with imposed periodic boundary conditions of Peng *et al.*[23] suggest an extremely large metal-to-graphene charge transfer in the Fe-adatom graphene system, a value that is eight times that suggested by Duffy and Blackman; they do not however report values for the binding energies of the Fe atoms to the various sites found on graphene/graphite. There

TABLE I. The spin-orbital occupancies for the free atom.

Metal	$s(\alpha,\beta)$	$d_{z^2}(\alpha,\beta)$	$d_{xz}(\alpha,\beta)$	$d_{yz}(\alpha,\beta)$	$d_{x^2-y^2}(\alpha,\beta)$	$d_{xy}(\alpha,\beta)$	Electronic configuration
Fe	0.99,0.64	0.99,0.11	0.99,0.53	0.99,0.25	0.99,0.29	0.99,0.18	$3d^{6.32}4s^{1.64}$
Co	1.00,0.36	1.00,0.76	1.00,0.53	1.00,0.19	1.00,0.54	1.00,0.62	$3d^{7.62}4s^{1.36}$
Ni	1.00,0.23	1.00,1.00	1.00,0.83	1.00,0.32	1.00,0.87	1.00,0.76	$3d^{8.77}4s^{1.23}$
Pt	1.00,0.00	1.00,0.88	1.00,0.82	1.00,0.68	1.00,0.97	1.00,0.66	$3d^{9.01}4s^{1.00}$

is thus a range of different values calculated for the binding energies.

In this paper, we present density functional theory calculations of Fe, Co, and Ni adatoms and both homonuclear and heteronuclear dimers adsorbed on graphene. We considered the following heteronuclear dimers: FeCo, FeNi, CoNi, FePt, CoPt, and NiPt. Thus we all cover all combinations of Fe, Co, and Ni, and Pt is included because it is interesting to investigate how the magnetic moments of clusters containing metals that are ferromagnetic in the bulk phase are modified when bonded with a metal that is nonmagnetic in the bulk phase. In addition Pt is an important catalytic metal and thus investigating the electronic structure of heteronuclear clusters containing Pt would be interesting. Various adsorption sites are considered for both the adatom and dimers, with various configurations considered in the case of the dimers. Two dimer configurations, with the dimer bond axis perpendicular to the graphene plane, that were not considered in previous work are studied here as well. The binding and atomization energies give us a direct indication of the type (e.g., chemisorbed or physisorbed) of metal-graphene interaction. Furthermore, by comparing the magnetic moments and bond lengths (only in the dimer case) of the bound adatoms and dimers to the case where they are unbound or free, we can elucidate the feasibility of using graphene as a support material for these clusters. Electron population analysis is also done for our further understanding of the cluster-graphene interaction. We show in this paper that, compared to their unbound states, the dimers have very similar magnetic moments, metal-metal bond lengths, and energies. The small metal-to-graphene charge transfer and the low binding energies suggest a weak but finite interaction between metal and graphene, suggestive of physisorption. Extensive convergence testing was first carried out to justify the choice of certain calculational parameters. These are presented in Sec. II.

II. COMPUTATIONAL METHOD AND CALIBRATION

The plane-wave based density functional theory program PWSCF (ESPRESSO Version 3.2) was used to perform all calculations.[37] The Rappe-Rabe-Kaxiras-Joannopoulos (RRKJ) ultrasoft pseudopotential with nonlinear core correction[38] was used for all species (i.e., C, Fe, Co, and Ni) with the Perdew-Burke-Ernzerhof (PBE) generalized gradient approximation (GGA) correction[39] formalism employed for the exchange-correlation functional. All pseudopotentials were obtained from the PWSCF pseudopotential online reference.[40] Smearing was used to aid convergence. Specifically, we made use of the Marzari-Vanderbilt method[41] or cold smearing with a small Gaussian spread of 0.001 Ry or 0.013 eV. The magnetic moments are particularly sensitive to the smearing width used. We find that for an Fe adatom above a hole site [see Fig. 2(a)], the change in adatom binding energy for a change in smearing from 0.001 Ry and 0.03 Ry is 0.05 eV; all other parameters remain constant. The magnetic moment obtained when a smearing width of 0.001 Ry was used is $2.00\mu_B$, while the magnetic moment obtained when a width of 0.03 Ry was used is $2.20\mu_B$. Localized electron population analysis was carried out by integrating the projected density of states. This was useful in assigning local charges and local magnetic moments on the atoms.

Relative to the main group elements, the ground state properties of the transition metals (e.g., binding energies, bond lengths, and electronic state) are particularly sensitive on to how the exchange-correlation interaction is treated.[2,4,5,18,19,42–44] This is a result of the complex $3d$-$4s$ exchange-correlation interactions arising from the fact that these energy states lie close to each other. One way around this problem is to make use of a multideterminant wave function (e.g., a configuration interaction calculation). A less computationally expensive choice would be to adopt a pseudopotential that treats the exchange-correlation interaction better. Harris and Jones[45] showed that the local spin-density approximation (LSDA) for the exchange-correlation functional favors d occupancies (by approximately 1 eV) relative to the GGA framework. We used the RRKJ ultrasoft pseudopotential constructed with electron configuration $4s^13d^{n-1}$. The spin-orbital occupancies of the free atoms are given in Table I. We calculated this configuration for a supercell of dimension $9.84\times9.84\times14.76$ Å^3 using cutoff energies of 40 Ry for the wave function and 480 Ry for the electron density.

It has been shown[2,3,18,44] that for small transition metal clusters of Fe, Co, and Ni, the projected electron configurations are in between the $4s^13d^{n-1}$ and $4s^23d^{n-2}$ states. Moroni *et al.*[44] pointed out that GGA- and LSDA-type calculations are poor in predicting the ground state electronic structure of the free atoms ($4s^23d^{n-2}$) partly because of the inadequate treatment of exchange correlation in the functionals used.[46,47] Using either all-electron calculations or ultrasoft pseudopotential calculations, Moroni *et al.* found that the free Fe, Co, and Ni atoms have electronic configurations $3d^{6.2}s^{1.8}$, $3d^{7.7}4s^{1.3}$, and $3d^{9.0}s^{1.0}$, respectively. The occupancies we have obtained are similar (see Table I). The problem with the preference of d occupancy over s occupancy is that if these atoms are involved in systems where the s-state occupancy is lower relative to the free-atom case (e.g., in a cluster or when bound to a surface), the binding energies predicted would be

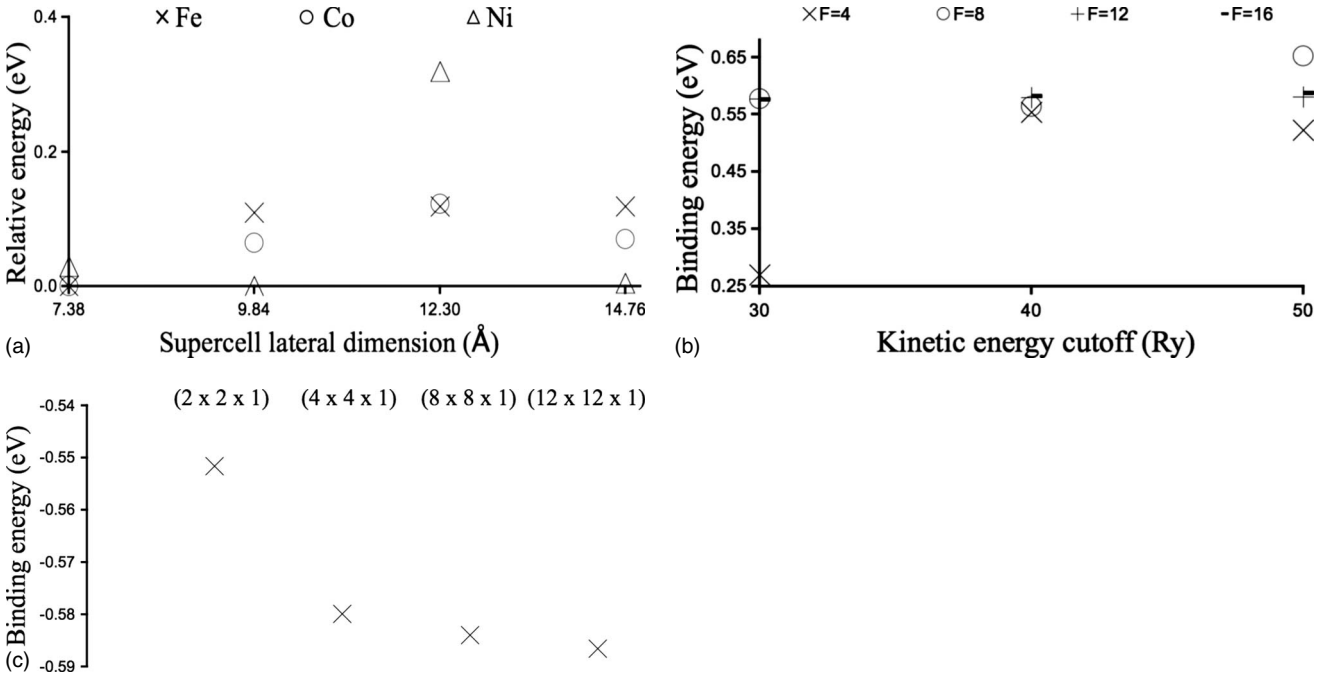

FIG. 1. Convergence testing: (a) the total energies of the Fe, Co, and Ni atoms taken relative to the minimum total energy in each set as a function of the lateral dimension of the supercell (in multiples of the unit cell of graphene, 2.46 Å) using 40 and 480 Ry for the wave function and electron density cutoffs, respectively. (b) Dependence of the binding energy of an Fe adatom adsorbed at a hole site on the wave function and electron density cutoffs. The electron density cutoff is given as $F\times$ (wave function cutoff). (c) Binding energy of an Fe adatom as a function of the Monkhorst-Pack grid used. Note that in all cases, a Marzari-Vanderbilt smearing width of 0.001 Ry and a force convergence threshold of 0.001 a.u. were used.

underestimated. The binding energies, magnetic moments, bond lengths, and electronic configurations predicted in this work are taken with reference to atoms with the calculated ground state electronic configurations given in Table I. We note that Hund's rule is still obeyed in that the free Fe, Co, Ni, and Pt atoms have magnetic moments of $4\mu_B$, $3\mu_B$, $2\mu_B$, and $2\mu_B$, which correspond to the maximum spin multiplicity for each atom. We therefore expect no problems in terms of predicting magnetic moments. In the case of carbon, the usual $2s^2 2p^2$ state is used for which there is no known problem.

We checked the following parameters for convergences: the size of the supercell, the kinetic energy cutoff, the cutoff for electron density, the number of k points for sampling the Brillouin zone, and the force convergence threshold. We describe our convergence calibration methodology here. We checked for interactions of the system with its periodic images using vacuum thicknesses of 12.4 and 17.4 Å. For these vacuum thicknesses, the Fe-adatom binding energies differ by 0.005 eV and therefore we made use of a vacuum thickness of 12.4 Å for all our calculations. The results of the calibration for the lateral dimensions of the supercell are shown in Fig. 1(a). A 4×4 supercell was found to be adequate. This supercell size was also used in previous work.[6,17]

Convergence with respect to cutoff energies for both the wave function and the electron density was checked by calculating the binding energy of an Fe adatom adsorbed at the hole site. The results for the binding energies are shown in Fig. 1(b). For the carbon pseudopotential used in this work, convergence is obtained for 30–32 and 200–240 Ry for these cutoff energies.[48] For the Fe, Co, and Ni pseudopotentials, a wave function cutoff energy of 40–50 Ry has been proposed[38] and we find that appropriate cutoff energies to use are 40 and 480 Ry. In calibrating these cutoff energies, we used a force convergence threshold of 10^{-3} a.u. and a $(4\times4\times1)$ Monkhorst-Pack grid.[49] We did not use any Brillouin zone shift. Changing the force convergence threshold to 10^{-4} a.u. changed the Fe-adatom binding energy by less than 10^{-3} eV. In Fig. 1(c) we show the results of Brillouin zone sampling. We used a $(8\times8\times1)$ Monkhorst-Pack grid in our calculations.

III. RESULTS

This section consists of three subsections. The first discusses Fe, Co, and Ni atoms adsorbed on graphene. An important motivation for Sec. III A is to allow us to compare our methodology against the results of previous work. Section III B discusses results for homonuclear Fe, Co, and Ni dimers adsorbed on graphene. This provides the reference point for the discussion of the heteronuclear clusters in Sec. III C.

A. Adatoms

The two high-symmetry adsorption sites illustrated in Fig. 2 were investigated. Configuration 1.1 [Fig. 2(a)] consists of a metal atom adsorbed above a hole site and configuration

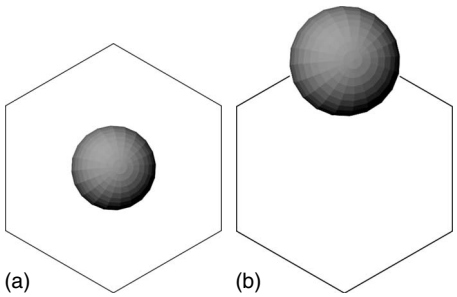

FIG. 2. Schematic illustration of the adsorbed adatom configurations (top view): (a) adatom above a hole site and (b) adatom atop a carbon atom or above an atom site. The hexagon represents the six nearest carbon atoms found in the graphene layer.

1.2 [Fig. 2(b)] consists of a metal atom adsorbed above a carbon atom. The bridge site, where a metal atom is adsorbed atop the midpoint of a carbon-carbon bond, is not considered in this work. Unlike graphite, all carbon sites are equivalent; there are no alpha- or beta-carbon sites. The binding energies (E_b), magnetic moments (M), bond lengths (L), charge transfers (q), and population analyses from our calculations are summarized in Table II.

The binding energies from our calculations suggest that the metal adatoms are physisorbed on graphene. In comparison to the results of previous work, we find binding energies that are significantly smaller (see Table II). We note that the differences in binding energies relative to previous work are much larger than any convergence errors (<0.01 eV) in our calculations. The differences in the adatom binding energy between our calculations and the results in Refs. 6 and 7 are likely to be due to the choice of the basis functions and the exchange-correlation functional used. Duffy and Blackman[7] used a double-numeric basis set augmented by polarization functions, while the calculations by Yagi *et al.*[6] and our calculations here use plane waves with cutoff energies of 21.1 and 40 Ry, respectively. To estimate the exchange-correlation energy, Duffy and Blackman used the Slater-Vosko-Wilk-Nusair functional while Yagi *et al.* used the PW91 functional. We used the PBE functional here. Previous work has shown that the LSDA does not adequately treat electronic configuration of the free atom and thus overestimates the binding energy. The electronic configurations and thus binding energies are much better calculated using generalized gradient correction functionals. The overestimation of the binding energy arises[46,47] from an underestimation of the interconfigurational energies, which is the energy required to go from one electronic configuration to another. This explains the rather large binding energies obtained by Duffy and Blackman relative to both our work and the work of Yagi *et al.* We expect lower binding energies than the results calculated here if the interconfigurational energies are treated with a higher degree of accuracy.

There are three differences between our calculations and the calculations by Yagi *et al.* We used the PBE functional, wave function cutoff energy of 40 Ry, and a RRKJ ultrasoft pseudopotential, while Yagi *et al.*[6] used the PW91 functional, a wave function cutoff energy of 21.1 Ry, and a Kresse-Furthmüller ultrasoft pseudopotential. We do not expect the use of these similar exchange-correlation functionals to account for the differences of 0.4, 0.6, and 0.1 eV for Fe, Co, and Ni adatom adsorption energies, respectively. We checked the effect of the cutoff energies by calculating the Fe adatom above the hole site adsorption energy at wave function cutoff energy of 21 Ry with density cutoff energies of 84, 168, and 252 Ry obtaining values of 0.13, 0.54, and 0.57 eV, respectively. Compared to the adsorption energy of 0.58 eV obtained using cutoff energies of 40 Ry for the wave function and 480 Ry for the density, these results suggest that the difference in our calculations and those in Ref. 6 are not due to the difference in the wave function cutoff energy. We note that the density cutoff energy is not reported in Ref. 6. In comparison with Ref. 50, we used the same exchange-correlation functional and very similar wave function cutoff energy. They used 44 Ry and we used 40 Ry for the wave function cutoff energy, and given our calibration calculations at different cutoff energies, we do not expect the differences to arise from this. We note that their adatom adsorption energy for Fe above a hole site (1.42 eV) is higher than their adatom adsorption energy for Co above a hole site (1.32 eV). This is opposite to the relative adsorption energies calculated

TABLE II. Data for Fe, Co, and Ni adatom adsorption on graphene: the binding energies (E_b), the magnetic moments (M), the metal-to-graphene plane distance (L), the metal-to-graphene charge transfer in units of electrons (q), and the electronic configuration of the metal atoms when bound in the respective configurations.

		E_b (eV)			M (μ_B)			L (Å)			q			Electronic configuration		
Configuration		a	b	c	a	b	c	a	b	c	a	b	c	a	b	c
Fe	1.1	0.58	2.0	0.99	2.0	2.0	2.1	1.54	1.52	1.51	0.7	0.2		$3d^{7.16}4s^{0.15}$	$3d^{7.2}4sp^{0.6}$	
	1.2	0.25	1.3		4.2			2.21			0.3			$3d^{6.57}4s^{1.08}$		
Co	1.1	0.97	2.4	1.58	1.0	1.0	1.0	1.51	1.52	1.49	0.6	0.2		$3d^{8.25}4s^{0.15}$	$3d^{8.2}4sp^{0.6}$	
	1.2	0.44	1.9		2.8			2.10			0.3			$3d^{7.79}4s^{0.93}$		
Ni	1.1	1.37	2.5	1.53	0.0	0.0	0.0	1.55	1.53	1.52	0.7	0.2		$3d^{9.12}4s^{0.16}$	$3d^{9.2}4sp^{0.6}$	
	1.2	0.96	2.1		0.0			1.81			0.6			$3d^{9.18}4s^{0.25}$		

[a]This work: plane-wave pseudopotential DFT calculations using the PBE form of the GGA of the exchange-correlation functional.
[b]Duffy and Blackman: double-numeric basis set linear combination of atomic orbitals-based DFT calculations using the VWN parametrization for the LSDA of the exchange-correlation functional (Ref. 7).
[c]Yagi *et al.*: plane-wave pseudopotential DFT calculations using the PW91 form of the GGA of the exchange-correlation functional (Ref. 6).

by us, Yagi *et al.*,[6] and Duffy and Blackman.[7] Given that they used a different pseudopotential (Vanderbilt ultrasoft), we think that the electron configuration used by Mao *et al.*[50] for the free Fe and Co atoms is not close to those we obtained. As discussed above, the calculated adsorption energy is very sensitive to the projected electronic configuration on the metal atom and this is likely to be the reason for the differences in the calculated adsorption energies.

The increase in binding energy from Fe to Co to Ni results from a corresponding decrease in the interconfigurational energy. The experimental interconfigurational energies of Fe, Co, and Ni, for the transfer of one electron from an *s* orbital to a *d* orbital, i.e., $3d^{n-2}4s^2 \rightarrow 3d^{n-1}4s^1$, are 0.87, 0.42, and −0.03 eV, respectively (see Ref. 43 and references therein). Table II shows the respective electronic configurations of the adatoms when bound to graphene. Apart from Fe and Co adatoms bound as configuration 1.2, there is significant change in the electronic configurations of the adatoms relative to their free atomic state (see Table I). As Fe requires the greatest energy per unit charge transferred from an *s* orbital to a *d* orbital while Ni requires the least energy (in fact, favoring a higher occupancy of the *d* orbitals although to just a small extent), Fe bonds weakest to graphene while Ni bonds strongest regardless of the geometrical configuration.

We find that the occupation of the carbon p_z orbitals is increased with adsorption and therefore conclude that there is charge transfer from the metal atom to the π bonds of graphene. We find almost no change in the electron density projected onto the *s*, p_x, and p_y orbitals of the carbon atoms; we conclude that there is little charge transfer to the σ bonds of graphene. It is interesting to note that the metal-to-graphene charge transfer calculated by Duffy and Blackman is almost three times that calculated in this work. The main discrepancy between our work and that of Duffy and Blackman lies in the occupancy of the *s* (and *p*) orbitals of the metal atoms. The metal-to-graphene separation and magnetic moment are in good agreement with previous work.[6,7]

The decrease in magnetic moment by $2\mu_B$ when the metal adatom is bound above a hole site (i.e., configuration 1.1) stems from the fact that the *s* states are raised above the Fermi level. This is evident in Fig. 3. If we refer to an electronic configuration of either $4s^13d^{n-1}$ or $4s^23d^{n-2}$, we see that the pairing of the electron(s) that previously occupied the *s* states with the *d*-state electrons would result in a decrease of exactly $2\mu_B$ (see Table II). This is consistent with the findings of Duffy and Blackman.[7]

In the case where Fe and Co adatoms are bound directly above a carbon atom (i.e., configuration 1.2), the $s(\alpha)$ state is still found below the Fermi level while the $s(\beta)$ state is found above it where α and β refer to the majority (spin-up) and minority (spin-down) spins, respectively. The electrons are redistributed among the *d* states, particularly the d_{z^2} state in the case of Fe and the d_{z^2} and d_{yz} states in Co. This leads to an interconfigurational change, where an electron from the *s* orbital is transferred to a *d* orbital, with no change in the net magnetic moment of the atom. In the case of Ni however, the situation is the same as when the metal atom is found above a hole site, viz., both the *s* states are now above the Fermi level and the pairing of the electrons that previously occupied these states with those in the *d* states results in a decrease of $2\mu_B$ for its magnetic moment. Again we can understand why Ni is more likely to promote electrons from *s* to *d* states because its interconfigurational energy is exothermic, unlike Fe and Co for which this energy is endothermic.

In our calculations, spin-polarized bands are found for Fe and Co but not for Ni. The magnetic moments are localized on the metal adatoms with rather small contributions from graphene (see Table III). While we predict a small magnetic moment localized on graphene, Duffy and Blackman[7] found no magnetic moment associated with graphene. As opposed to being semimetallic as was the case in pure graphene [see Fig. 4(a)], the band structures shown in Fig. 5 indicate that these systems are now semiconducting. In their study of the adsorption of hydrogen on graphene,[51] Duplock *et al.* reasoned that the presence of an adatom ionic core would break the symmetry of any periodic potential thereby opening up a gap changing the graphene from being semimetallic to semiconducting. We expect that the metal adatom has the same effect as the H adatom. Of particular interest is the gap (both between states of different spin and states of the same spin) that is opened up at high-symmetry point *K* in the irreducible wedge of the Brillouin zone. The various interesting electronic properties of graphene (and graphite) stem from the form of the bands at and near this point, i.e., the Dirac cone centered at point *K*. However with metal adatoms on graphene, the Dirac cone no longer exists. Thus transition metal adsorption might have implication for the relativistic properties of graphene. Nonetheless, the band gaps that arise are of potential interest in spintronic device application.

B. Homonuclear dimers

Four high-symmetry bound dimer configurations were identified for geometry optimization. These are shown in the schematic given in Fig. 6. Previous work[6,7] that dealt with dimer adsorption on graphene only focused on configurations 2.1 and 2.2. Given the weak adatom-graphene interaction, we postulated that dimers in either configuration 2.3 and/or 2.4 might be more stable.

It is instructive that analysis of the bound dimers be done alongside analysis of the free dimers. The objective here is twofold. First, the results of our free dimer calculations are compared to previous work. Given that much more work has been on free dimers, this comparison allows a gauge accuracy of our calculations. Second, as we are interested in the effect of graphene as a support material and the relative stabilities of the various dimer configurations when bound to graphene, direct comparison of the bound dimer atomization and binding energies and magnetic moments and bond lengths with those of the free dimers allows us to determine the effect that graphene has on these dimers when bound. Data for the bond energies and magnetic moments for the free Fe, Co, and Ni clusters are given in Tables IV–VI, respectively. Corresponding data from previous work are also given.

The level of theory applied in determining the bond dissociation energies of the free Fe, Co, and Ni dimers is clearly inadequate (see Tables IV–VI). The free dimer bond dissociation energies that we have calculated differ from experi-

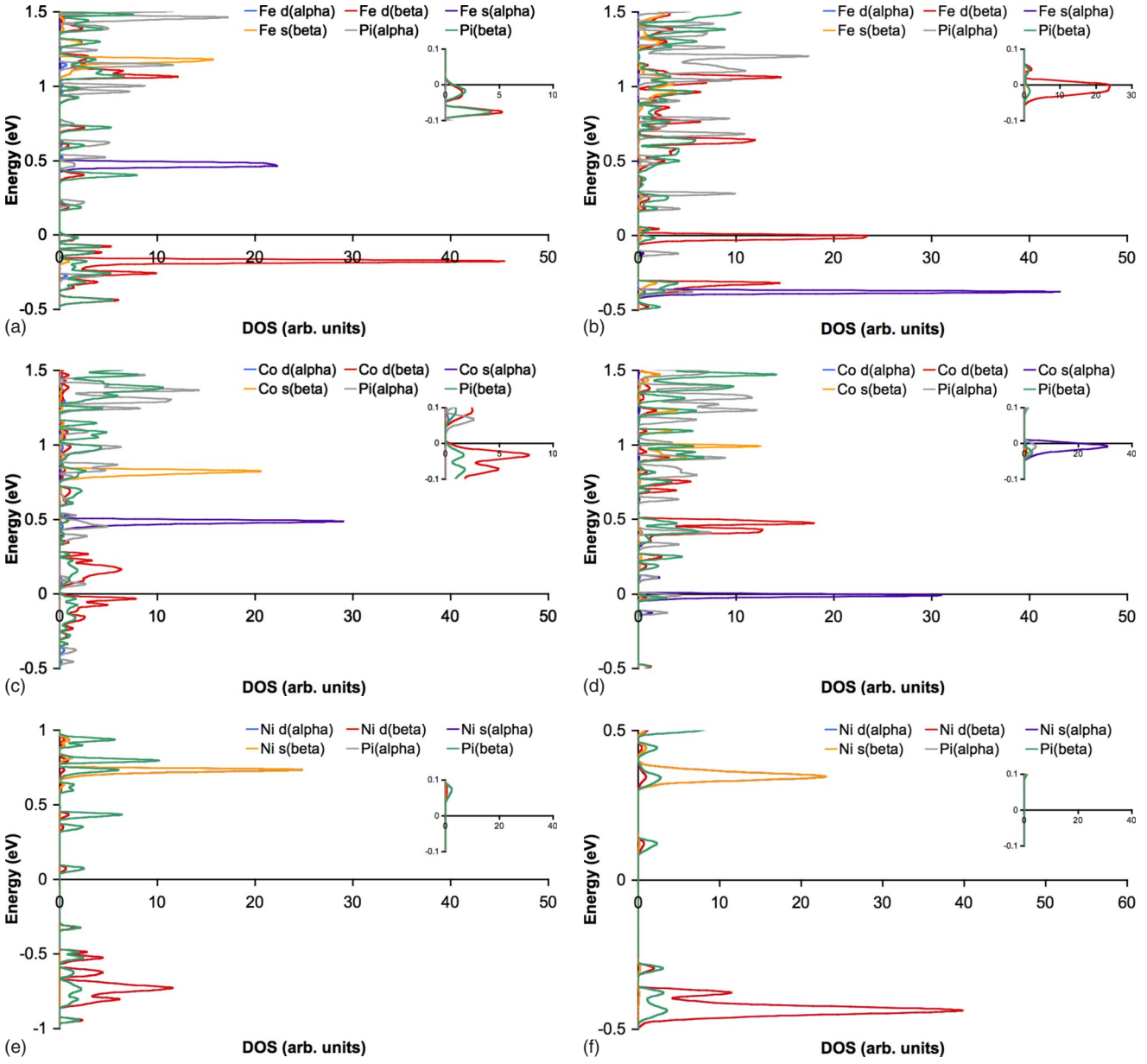

FIG. 3. (Color online) The projected density of states for configurations (a), (c), and (e) 1.1 and (b), (d), and (f) 1.2 for Fe, Co, and Ni. The Fermi level is referenced at 0 eV. Alpha and beta refer to the majority (spin-up) and minority (spin-down) spin states, respectively. The alpha and beta density of states overlap exactly in (e) and (f). The raising of both *s* spin states above the Fermi level in (c), (e), and (f) results in a decrease of $2\mu_B$ for the magnetic moment of Fe, Co, and Ni when bound as configuration 1.1 (above a hole site) and of Ni when bound as configuration 1.2 (above an atom site). Only the beta (minority or spin-down) *s* states are raised above the Fermi level in (b) and (d) which results in little change in the magnetic moment of Fe and Co when bound as configuration 1.2 (above an atom site). Insets zoom in on the density of states within 0.1 eV of the Fermi level.

ment by between 0.50 (Ref. 54) and 0.58 (Ref. 55) for the Fe dimer, 0.63 (Ref. 57) and 0.67 (Ref. 56) for the Co dimer, and 0.29 (Ref. 58) for the Ni dimer, in units of eV/atom. The overestimation of this energy largely stems from the exchange-correlation functional used. For example, depending on the exchange-correlation functional used, the bond dissociation energy of the Fe dimer can range from 0.55 to 1.55 eV. The form of the PW91 exchange-correlation functional is closest to that of the PBE exchange-correlation functional that we have used in our calculations here. Even so, we find from the PW91 calculations of Yanagisawa *et al.*[43] that there is still a difference of 0.33, 0.03, and 0.15 eV/atom for the Fe, Co, and Ni dimer bond dissociation energies, respectively. Our results are closer to calculations based on the Becke exchange one-parameter progressive correlation functional.

The importance of the exchange-correlation functional in predicting the bond dissociation energies largely stems from how well the functional treats interconfigurational change (e.g., $3d^{n-2}4s^2 \rightarrow 3d^{n-1}4s^1$) and therefore how well it estimates the interconfigurational energy. As mentioned, the LSDA functional form for exchange correlation has been

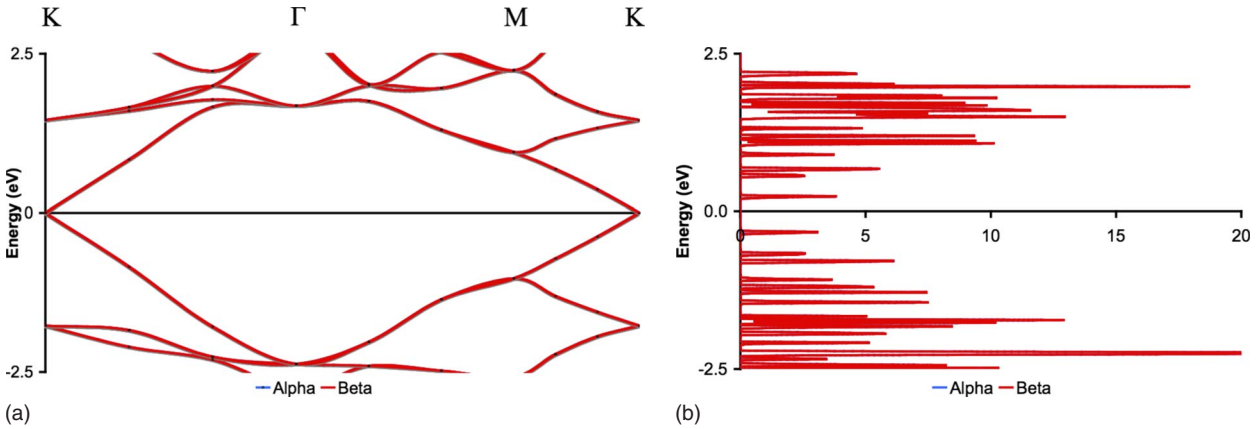

FIG. 4. (Color online) Band structure and density of states for graphene as calculated in this work.

shown[2,18] to be poor in predicting the dimer bond dissociation energy. Jeng and Hsue[46] and Kutzler and Painter[47] found that the use of LSDA underestimates the interconfigurational energy relative to GGA and ultimately relative to experimental data. This then results in an overestimation of the bond dissociation energy. As mentioned in Sec. III A, the Fe, Co, and Ni atoms in their respective dimers prefer atomic configurations that are "between" the states with electronic configurations of $3d^{n-2}4s^2$ and $3d^{n-1}4s^1$. We found that the free Fe, Co, and Ni dimers have atoms with localized atomic electronic configurations $3d^{6.92}4s^{1.04}$, $3d^{7.92}4s^{1.05}$, and $3d^{8.97}4s^{1.05}$, respectively. These configurations are very close to the $3d^{n-1}4s^1$ configuration and are not quite between the $3d^{n-2}4s^2$ and $3d^{n-1}4s^1$ states. This is possibly because little energy is required to induce the interconfigurational change therefore overestimating the bond dissociation energies. Aside from the exchange-correlation functional form, the potential that is used to describe the free atom is important as well. Castro and Salahub[18] and Jamorski *et al.*[2] showed that the use of a nonlocal potential as well as a nonsymmetric atomic electronic state gives a better estimate of the dimer bond dissociation energies.

The electronic configurations of the Fe, Co, and Ni dimers were found to be the following:

$$\{^7\Delta_u(1\sigma_\alpha 1\pi_\alpha 1\pi_\alpha 1\delta_\alpha 1\delta_\alpha 1\delta_\alpha^* 2\sigma_\alpha 1\sigma_\beta 1\delta_\alpha^* 1\pi_\alpha^* 1\pi_\alpha^* 2\sigma_\alpha^* 1\pi_\beta 1\pi_\beta 2\sigma_\beta 1\delta_\beta)\},$$

$$\{^5\delta_g(1\sigma_\alpha 1\pi_\alpha 1\pi_\alpha 1\sigma_\beta 1\delta_\alpha 2\sigma_\alpha 1\delta_\alpha 1\delta_\alpha^* 1\pi_\alpha^* 1\pi_\alpha^* 1\pi_\beta 1\pi_\beta 2\sigma_\alpha^* 2\sigma_\beta 1\delta_\alpha^* 1\delta_\beta 1\delta_\beta 1\delta_\beta^*)\},$$

$$\{^3\Sigma(1\sigma_\alpha 1\pi_\alpha 1\pi_\alpha 1\sigma_\beta 1\pi_\alpha^* 1\pi_\alpha^* 2\sigma_\alpha 1\pi_\beta 1\pi_\beta 2\sigma_\beta 1\delta_\alpha 1\delta_\alpha 2\sigma_\alpha^* 1\delta_\alpha^* 1\delta_\alpha^* 1\delta_\beta 1\delta_\beta 2\sigma_\beta^* 1\delta_\beta^* 1\delta_\beta^*)\}.$$

This implies total magnetic moments of $6\mu_B$, $4\mu_B$, and $2\mu_B$ for the Fe, Co, and Ni dimers, respectively. The electronic states (though not the exact electronic configuration) thus determined are in excellent agreement with almost all of the previous calculations done on these dimers (see Refs. 18, 43, and 53 for Fe,[2,43] for Co, and[43] for Ni). The bond lengths are also in very good agreement with both theoretical calculations as well as from experimental data.

The binding energies, magnetic moments, metal-metal bond lengths, and metal-graphene separation distances that we have calculated for the configurations 2.1 and 2.2 for all three metals are in excellent agreement with the work of Yagi *et al.*[6] The main discrepancy between their work and the present work is the energy required to atomize the bound dimer. This stems from the values used for the bond dissociation energies of the free dimers which have been shown (see Tables IV–VI) to be extremely sensitive to the form of the exchange-correlation functional used in the calculation. The free dimer bond dissociation energies that we have calculated differ from those determined by Yagi *et al.* by 0.41, 0.60, and 0.22 eV/atom for the Fe, Co, and Ni dimers, respectively. Yagi *et al.* used of the PW91 functional while we

TABLE III. Local magnetic moments for the adatoms and the graphene.

Configuration		Adatom (μ_B)	Graphene (μ_B)
Fe	1.1	2.23	−0.19
	1.2	4.18	0.01
Co	1.1	1.13	−0.12
	1.2	2.73	0.06
Ni	1.1	0.00	0.00
	1.2	0.00	0.00

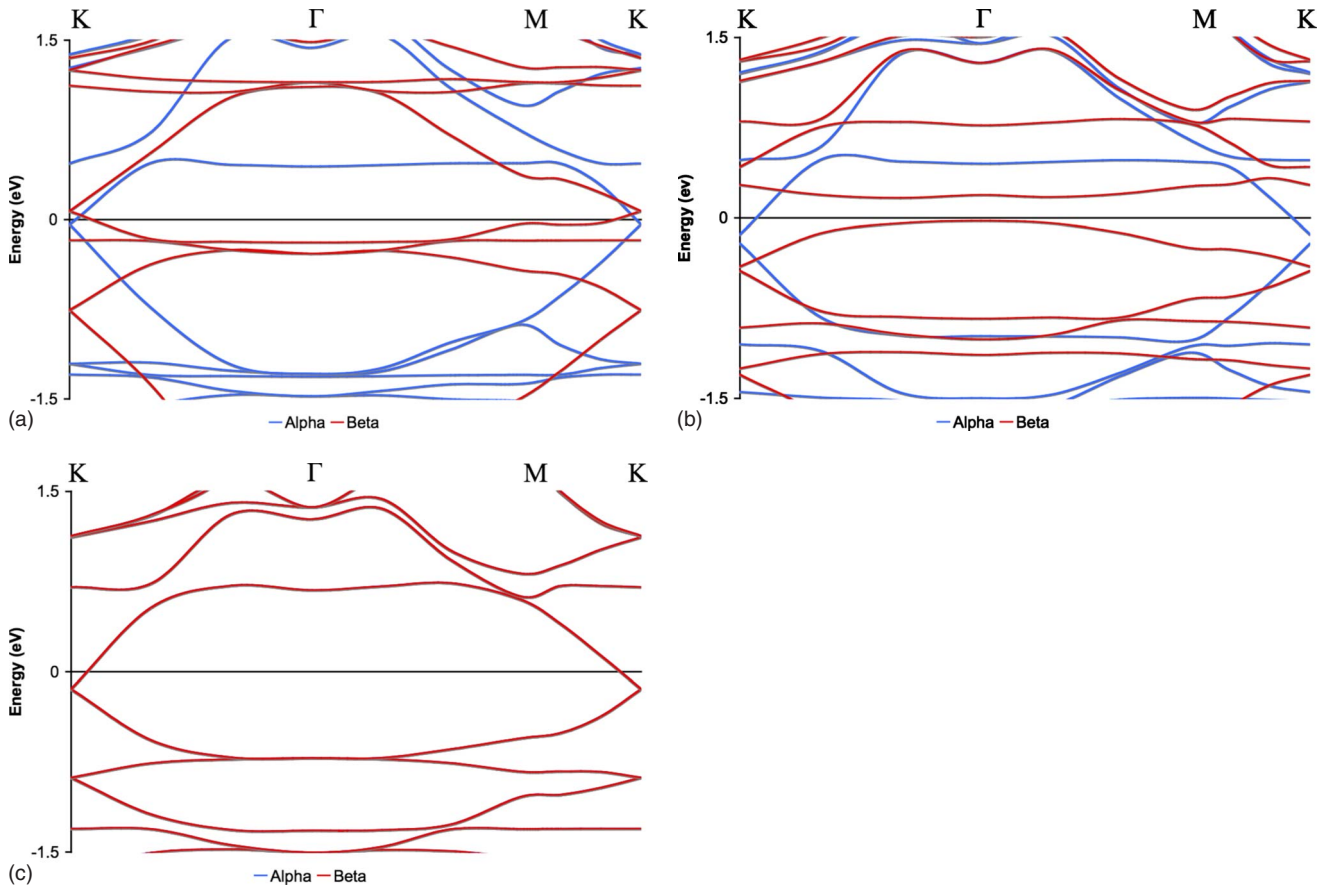

FIG. 5. (Color online) (a)–(c) Band structures for Fe, Co, and Ni when bound as configuration 1.1 (above a hole site), i.e., the more stable adatom configuration. The spin bands overlap exactly in the case of Ni.

used of the PBE functional. As mentioned previously, though both of these are generalized gradient approximations to the exchange-correlation electron interaction and are fairly close in their form, we see that the atomization energy (of the metal dimer from the graphene surface) values can differ by as much as 0.60 eV/atom. Relative to the work of Duffy and Blackman, we obtain similar magnetization, metal-metal bond lengths, and metal-to-graphene separation distances although they used the LSDA to exchange correlation. Again, as with the adatom case, we predict a smaller metal-to-graphene charge transfer. For the Ni_2 dimer, however, at least between configurations 2.1 and 2.2, our calculations are in agreement with Yagi's results which show that configuration 2.2 is more stable while calculations of Duffy and Blackman predict what we have labeled as configuration 2.1 as being more stable (Table VII).

Our calculations show that the bound or adsorbed dimers retain almost all of their free cluster characteristics. This is seen by considering the bound dimers' bond length and total magnetic moment and is consistent with the weak binding

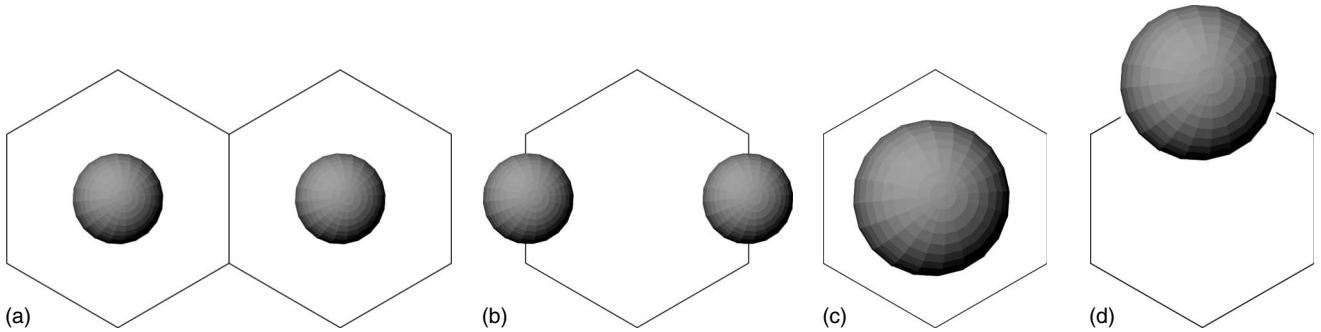

FIG. 6. Representation of the dimer configurations (top view): dimers above (a) two hole sites and (b) above two bridge sites with bond axes parallel to the graphene plane and dimers above (c) a hole site and (d) above an atom site with bond axes *perpendicular* to the graphene plane. Note that the spheres in (c) and (d) appear larger for the reason that the dimer is bound with its bond axis perpendicular to the graphene plane.

TABLE IV. Binding energy, magnetic moment, and bond length of the free Fe dimer.

Work	E_d (eV/atom)	M (μ_B/atom)	r_e (Å)
This work	1.15	3.0	1.96
Castro and Salahub[a]	4.38	3.0	1.96
Castro and Salahub[b]	1.04	3.0	1.96
Izquierdo *et al.*[c]	1.35	3.0	2.05
Izquierdo *et al.*[d]	1.55	3.0	1.99
Yanagisawa *et al.*[e]	1.25	3.0	2.03
Yanagisawa *et al.*[f]	0.69	3.0	2.66
Yanagisawa *et al.*[g]	0.75	3.0	2.08
Yanagisawa *et al.*[h]	1.48	3.0	2.01
Yanagisawa *et al.*[i]	0.55	3.0	2.52
Yanagisawa *et al.*[j]	1.59	3.0	2.06
Noro *et al.*[k]	0.79	3.0	2.06
Köhler *et al.*[l]	2.11	3.0	
Rohlfing *et al.*[m]		3.0	1.9
Moskovits *et al.*[n]	0.65		
Lian *et al.*[o]	0.57		

[a]LSDA results with respect to ^5D Fe atoms (Ref. 18).
[b]Nonlocal spin-density results with respect to nonspherical ^5D Fe atoms (Ref. 18).
[c]DFT (GGA for exchange correlation) with numerical atomic orbitals (single-zeta singly-polarized basis) and nonlocal pseudopotential for atomic core (Ref. 42).
[d]DFT (GGA for exchange correlation) with numerical atomic orbitals (double-zeta singly-polarized basis) basis) and nonlocal pseudopotential for atomic core (Ref. 42).
[e]Becke exchange one-parameter progressive correlation functional (Ref. 43).
[f]Hybrid Becke exchange Lee-Yang-Parr correlation functional (Ref. 43).
[g]Becke exchange (Ref. 43).
[h]Perdew-Wang 1991 exchange-correlation functional (Ref. 43).
[i]Second-order Møller-Plesset perturbation theory (Ref. 43).
[j]Full-electron configuration interaction molecular orbital theory (Ref. 43).
[k]Multireference self-consistent field and configuration interaction calculations (Ref. 52).
[l]Density functional based tight-binding calculation using linear combination of Slater-type orbitals (Ref. 1).
[m]Photoionization spectroscopy (Ref. 53).
[n]Resonance Raman spectroscopy (Ref. 54).
[o]Spectroscopic analysis using collision-induced dissociation of Fe_n with Xe (Ref. 55).

energy and the small amount of net charge transfer to the graphene. These data are presented in Fig. 7. The percentage change in the bound dimer's bond length with respect to the free case is a good indication of the extent to which graphene perturbs the dimer bond. These are presented in Table VIII. From these data we find that the change in bond length is greatest for configuration 2.1. For each of configurations 2.2, 2.3, and 2.4, there is less than a 10% change in the dimer bond length. We will further discuss this point later in this section.

TABLE V. Binding energy, magnetic moment, and bond length of the free Co dimer.

Work	E_d (eV/atom)	M (μ_B/atom)	r_e (Å)
This work	1.33	2.0	1.94
Jamorski *et al.*[a]	1.13	2.0	2.01
Jamorski *et al.*[b]	0.41	2.0	2.56
Yanagisawa *et al.*[c]	1.23	2.0	2.01
Yanagisawa *et al.*[d]	0.75	2.0	2.44
Yanagisawa *et al.*[e]	0.65	2.0	2.05
Yanagisawa *et al.*[f]	1.36	2.0	1.98
Yanagisawa *et al.*[g]	0.67	2.0	2.41
Yanagisawa *et al.*[h]	0.41	2.0	2.56
Hales *et al.*[i]	<0.66		
Russon *et al.*[j]	0.7–1.4		

[a]All-electron DFT calculation within GGA (Perdew-Wang gradient correction for exchange and Perdew correction for correlation), linear combination of Gaussian-type orbitals (Ref. 2).
[b]Limited configuration-interaction calculation (Ref. 2).
[c]Becke exchange one-parameter progressive correlation functional (Ref. 43).
[d]Hybrid Becke exchange Lee-Yang-Parr correlation functional (Ref. 43).
[e]Becke exchange (Ref. 43).
[f]Perdew-Wang 1991 exchange-correlation functional (Ref. 43).
[g]Second-order Møller-Plesset perturbation theory (Ref. 43).
[h]Multireference single- and double-configuration interaction molecular orbital theory (Ref. 43).
[i]Spectroscopic analysis of collision-induced dissociation of Co_n^+ using Xe (Ref. 56).
[j]Photodissociation measurements (Ref. 57).

The total magnetic moment of the dimer-graphene system is mainly localized on the metal atoms and relative to the free dimers; the bound dimers retain their magnetization except for the case where the Ni dimer is bound as configuration 2.1. When bound parallel to the graphene plane, the changes in electron population and magnetic moments are the same for both atoms. The exception to this is configuration 2.1 of Fe [see Fig. 7(a)]. In the particular case of Fe(2.1), slight buckling of the dimer bond is observed and is consistent with the work of Yagi *et al.*[6] As a result of this buckling, the two Fe atoms in configuration 2.1 have different localized magnetic moments and charges [see Fig. 7(a) and compare this to Figs. 7(e) and 7(i) for the Co and Ni 2.1 type configurations, respectively]. For the Ni dimer bound as configuration 2.1 [see Fig. 7(i)], the magnetization is completely quenched, just as in the case of the Ni adatoms. Where the bound dimer bond axis is perpendicular to the graphene plane (i.e., configurations 2.3 and 2.4), the metal atom closer to the graphene has the greater change in both its charge and magnetization. The metal atom located further from the graphene plane retains its free-atom-like properties to a greater extent suggesting that the metal atom closer to the graphene "shields" the former from the effect of graphene. Interestingly enough, the total magnetic moments are almost the same (within an error margin of less than

TABLE VI. Binding energy, magnetic moment, and bond length of the free Ni dimer.

Work	E_d (eV/atom)	M (μ_B/atom)	r_e (Å)
This work	1.31	1.0	2.08
Yanagisawa *et al.*[a]	1.34	1.0	2.13
Yanagisawa *et al.*[b]	0.98	1.0	2.30
Yanagisawa *et al.*[c]	0.96	1.0	2.18
Yanagisawa *et al.*[d]	1.46	1.0	2.10
Yanagisawa *et al.*[e]	0.935	1.0	2.27
Yanagisawa *et al.*[f]	0.90	1.0	2.24
Pou-Amérigo[g]	0.89		2.24
Michelini *et al.*[h]	1.67	1.0	2.07
Michelini *et al.*[i]	1.34	1.0	2.13
Morse *et al.*[j]	1.02		2.16

[a]Becke exchange one-parameter progressive correlation functional (Ref. 43).
[b]Hybrid Becke exchange Lee-Yang-Parr correlation functional (Ref. 43).
[c]Becke exchange (Ref. 43).
[d]Perdew-Wang 1991 exchange-correlation functional (Ref. 43).
[e]Second-order Møller-Plesset perturbation theory (Ref. 43).
[f]Complete active space second-order perturbation (Ref. 43).
[g]Multiconfigurational second-order perturbation theory calculations using atomic natural orbitals.
[h]DFT within the LSDA (VWN local correlation functional) using a triple-zeta STO basis set (Ref. 4).
[i]DFT within the GGA (PBE) using a triple-zeta STO basis set (Ref. 5).
[j]Resonant two photon ionization electronic spectroscopy analysis (predissociation limit) of the Ni_2 dimer (Ref. 58).

$0.1\mu_B$/atom) regardless of the configuration of the dimer.

The small binding energies again point toward a weak dimer-graphene interaction. The most stable Fe, Co, and Ni configurations (i.e., configuration 2.3) have binding energies of 0.36, 0.46, and 0.48 eV/atom, respectively, and atomization energies of 1.50, 1.79, and 1.79 eV/atom, respectively. There is a significant decrease in the binding energy per atom of the dimers relative to the most stable adatom configuration (i.e., configuration 1.1), with the Ni dimer showing the greatest percentage change. The dimer atomization energies are clearly higher than in the adatom case. This however stems primarily from the strength of the metal-metal bond and *not* from the interaction with the graphene *per se* as evidenced by both the small binding energies of the dimer to the graphene and the strength of the free Fe-Fe, Co-Co, and Ni-Ni bond dissociation energies of 1.15, 1.33, and 1.31 eV/atom, respectively.

Relative to the adatom case, the more stable dimer configurations (i.e., configurations 2.3 and 2.4) have a smaller amount of net metal-to-graphene charge transfer per metal atom. Again, there is a net increase in graphene's π-electron population and an insignificant change in its σ-electron population, pointing to some extent of hybridization of the metal atoms s and d_{z^2} orbitals with the graphenes delocalized π system. A small amount of net charge transfer to the graphene might possibly indicate that there is little change in the dimers' electronic state. Overall, the small change in bond length and the insignificant change in total magnetic moment with respect to when the dimers are free, the small binding energies and the small amount of charge transfer all point to a physisorbed state and we might expect that with increasing cluster size the free character of the bound cluster would also increase. This further validates the promise and potential of graphene as a suitable support material for small Fe, Co, and Ni clusters at least in context of their magnetic and catalytic capacities because it does not significantly change the electronic characteristics of the dimer.

The dimers bind more strongly when the dimer bond axis is perpendicular to the graphene plane. We find that the most stable dimer configuration with its bond axis parallel to the graphene plane is configuration 2.2 (consistent with previous work[6,7] except for the Ni dimer when compared to the results of Duffy and Blackman[7]) and the most stable dimer configuration with its bond axis perpendicular to the graphene plane is configuration 2.3. When we compare the binding energies

TABLE VII. Comparison of the atomization energy (E_{at}), binding energy (E_b), projected magnetic moments (μ_B), dimer bond lengths (Å), and charge transfer of the bound metal dimers for configurations 2.1 and 2.2 with the work of Duffy and Blackman and Yagi *et al.* The charge transfer again refers to the amount charge transferred from the metal dimer to the underlying graphene.

System		E_{at} (eV/atom)		E_b (eV/atom)		Magnetic moment (μ_B)			Dimer bond length (Å)			Charge transfer	
Work		a	c	a	c	a	b	c	a	b	c	a	b
Fe	2.1	1.31	1.75	0.16	0.19	3.47,3.06		3.5,3.1	2.27		2.22	0.38,0.44	
	2.2	1.38	1.83	0.23	0.27	3.20,3.20	3.0,3.0	3.2,3.2	2.11	2.09	2.11	0.34,0.34	0.1,0.1
Co	2.1	1.43	2.04	0.10	0.11	2.07,2.07		2.1,2.1	2.34		2.35	0.35,0.35	
	2.2	1.56	2.19	0.24	0.26	2.12,2.12	2.0,2.0	2.1,2.1	2.07	2.09	2.08	0.31,0.31	0.1,0.1
Ni	2.1	1.65	1.84	0.31	0.31	0.00,0.00	0.0,0.0	0.0,0.0	2.40	2.40	2.41	0.59,0.59	0.1,0.1
	2.2	1.68	1.85	0.33		0.99,0.98		1.0,1.0	2.24		2.24	0.36,0.36	

[a]This work.
[b]Duffy and Blackman (Ref. 7).
[c]Yagi *et al.* (Ref. 6).

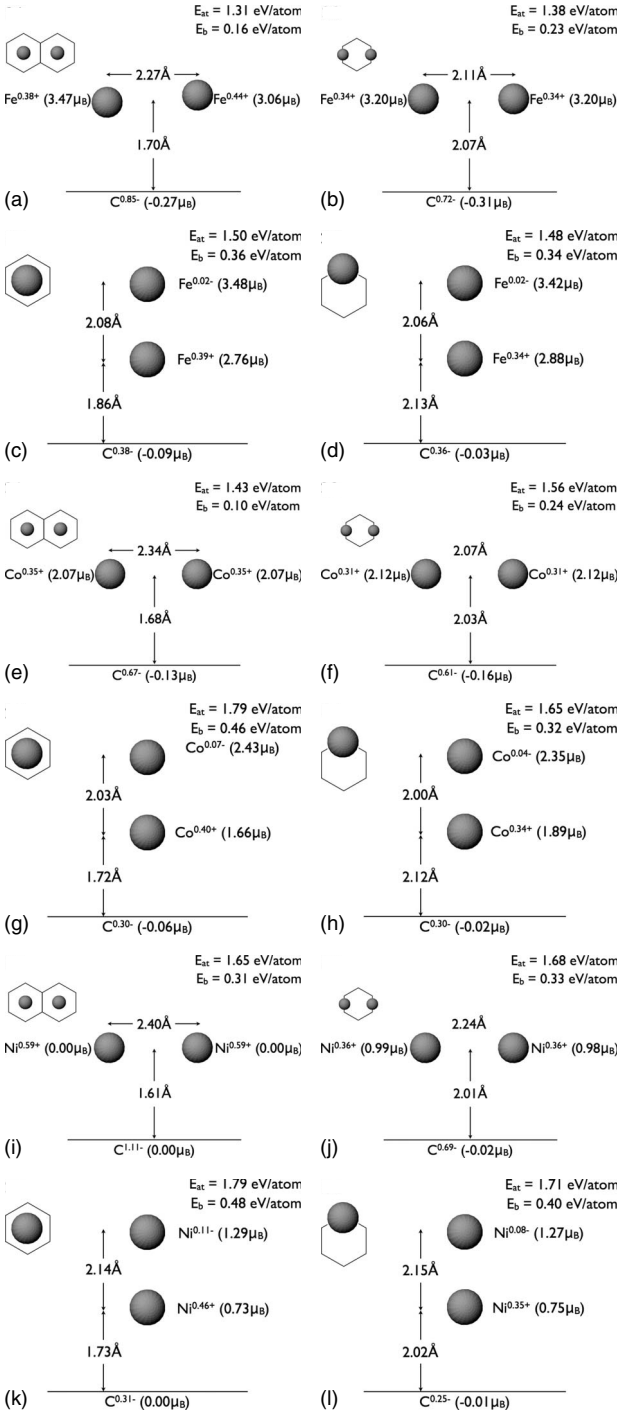

FIG. 7. Data for the bound dimers: [dimer species (dimer configuration)] (a) Fe(2.1), (b) Fe(2.2), (c) Fe(2.3), (d) Fe(2.4), (e) Co(2.1), (f) Co(2.2), (g) Co(2.3), (h) Co(2.4), (i) Ni(2.1), (j) Ni(2.2), (k) Ni(2.3), and (l) Ni(2.4). Inset in each subfigure's top left corner is a top view of that configuration as per shown in Fig. 6 (i.e., in the *x*-*y* plane). The main figure gives the side view (i.e., in the *x*-*z* plane). Shown in the figures are the atomization energies (E_{at}), the binding energies (E_b), the local charge on each species, the local magnetic moments, the projected electronic configuration, the bound dimer's bond length, and the average metal-to-graphene separation. Note that the baseline represents the graphene plane and C is a symbol used to represent the *whole* graphene plane and not just a single C atom found therein.

TABLE VIII. Percentage change in the bound dimers' bond lengths with respect to their respective unbound cases.

Conformer	2.1	2.2	2.3	2.4
Fe	15.82	7.65	6.12	5.10
Co	20.41	6.70	4.64	3.09
Ni	15.38	7.69	2.88	3.37

of these two types of configurations for each of the species, we find that the binding energies for configuration 2.3 is greater by 0.13, 0.22, and 0.15 eV than the respective binding energies of configuration 2.2 for each of Fe, Co, and Ni, respectively. When bound perpendicularly (i.e., bond axis is perpendicular to the graphene plane), the dimers characteristically have a much lower *total* charge transfer to the underlying graphene and a smaller percentage change in their metal-metal bond length relative to when bound parallel (i.e., bond axis is parallel to the graphene plane). A map of the electron density provides further evidence as to the extent to which the dimer is perturbed by the graphene, particularly its bond. As an example, we plot the isosurface of the Fe dimers' electron charge density (isovalue=0.06 a.u.). From Fig. 8 we see that there is a much greater decrease in the electron density between the two Fe atoms when bound as configuration 2.1 than in configurations 2.2, 2.3, and 2.4. This is less pronounced for configurations 2.2, 2.3, and 2.4. The weakening of the bond is evidenced by both the percentage change in bond lengths and the electron density isosurface plots.

The added binding strength of configurations 2.3 and 2.4 relative to configurations 2.1 and 2.2 results from the additional energy required for an interconfigurational change in the former. We refer the reader to the localized electronic configuration of the dimers (see Fig. 7). The free Fe, Co, and Ni dimers have atoms with electronic configurations of $3d^{6.92}4s^{1.04}$, $3d^{7.92}4s^{1.05}$, and $3d^{8.97}4s^{1.05}$, respectively. When bound as configurations 2.1 and 2.2, the electronic configurations of the metal atoms are very similar to their respective free dimer cases at least in terms of the *d*-electron configuration. The *s*-state occupancy is depleted to a large extent owing to the transfer of electrons from the *s* orbital to the graphene's π system. However, when bound as configurations 2.3 and 2.4, the metal atom that is farther from the graphene surface has an electronic configuration that is closer to the free atomic state rather than in the free dimer state. Therefore, removal of a dimer bound to graphene in configuration 2.3 or 2.4 requires input of energy not just to reverse the electron transfer from metal to graphene but also involves a change in the electronic configuration of one of the metal atoms. This therefore explains why more energy is required to remove the perpendicularly bound dimers relative to the ones bound parallel to the graphene.

The metal clusters prefer to agglomerate as dimers as opposed to remaining as separated adatoms. To quantify this, we consider the relative energy of a bound dimer to two isolated adatoms, viz., $\Delta E_{2\rightarrow(1+1)}=E(\text{bound dimer})-2E$ (most stable bound adatom) $+E$ (plain graphene sheet). The data for this are given in Table IX. The binding strengths,

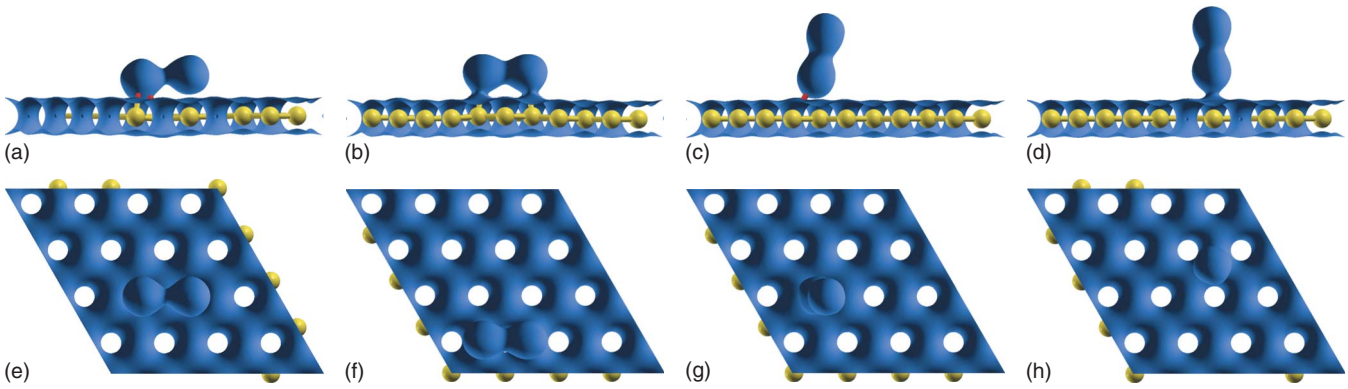

FIG. 8. (Color online) Electron density isosurface (isodensity value=0.06 a.u.) for the various bound Fe dimers. The weakening of the Fe-Fe bond in configuration 2.1 is well evidenced by the depreciation in electron density between the two atoms relative to the other cases. The pictures were generated using XCRYSDEN (Ref. 59).

$\Delta E_{2\rightarrow(1+1)}$, we have calculated show that the relative agglomeration tendency increases as Ni<Co<Fe. We point out to the reader that this simply accounts for the thermodynamics of adatom-to-dimer formation on the graphene surface; there are no kinetic data available at present to account for the rate at which these adatoms diffuse on the surface.

C. Heteronuclear dimers

We begin our discussion with analysis of the free dimers, FeCo, FeNi, CoNi, FePt, CoPt, and NiPt. The dimer bond dissociation energies and projected magnetic moments, charges and electron configurations, and bond lengths that we have calculated for these free dimers are presented in Fig. 9.

As with the homonuclear dimers, the accuracy of the calculated dimer bond dissociation energies depends strongly on how well the exchange-correlation functional used estimates the energy required for the interconfiguration change $3d^{n-2}4s^2 \rightarrow 3d^{n-1}4s^1$, viz., the interconfigurational energy.[43,60] Therefore, we expect that just like the homonuclear clusters, the binding energies that we have calculated are an overestimate since the interconfigurational energies have been underestimated. For the free FeCo, FeNi, and CoNi dimers, the bond energies that we have calculated are higher than those calculated by Gutsev *et al.* by 0.30, 0.14, and 0.25 eV, respectively. The methodology used by Gutsev *et al.* is quite different from that used here. They used the 6–311+G*/BPW91 level of theory in the GAUSSIAN98 program although they noted that the BPW91 and PBE exchange-correlation functionals provided rather similar results for the 3*d* homonuclear dimers. We therefore conclude that these differences in bond energies arise from the choice of basis functions.

The projected electronic configurations and magnetic moments and dimer bond lengths for the FeCo and CoNi dimers that we have calculated are in very good agreement with the values calculated by Gutsev *et al.* However for FeNi and FePt, the magnetic moments we calculated are $4.55\mu_B$ and $4.30\mu_B$, respectively, for a smearing of 0.001 Ry. This is because the highest occupied spin-up and spin-down single-particle states have eigenvalues that are very close to each other. Therefore, a zero smearing is required in order to ob-

TABLE IX. The relative binding strength for each of the bound dimer configurations relative to having two adatoms adsorbed at their respective most stable site (i.e., configuration 1.1—adatom above a hole site) for all of Fe, Co, and Ni.

	$\Delta E_{2\rightarrow(1+1)}$/eV			
Configuration	2.1	2.2	2.3	2.4
Fe	1.45	1.58	1.84	1.79
Co	0.93	1.19	1.65	1.36
Ni	0.57	0.62	0.84	0.70

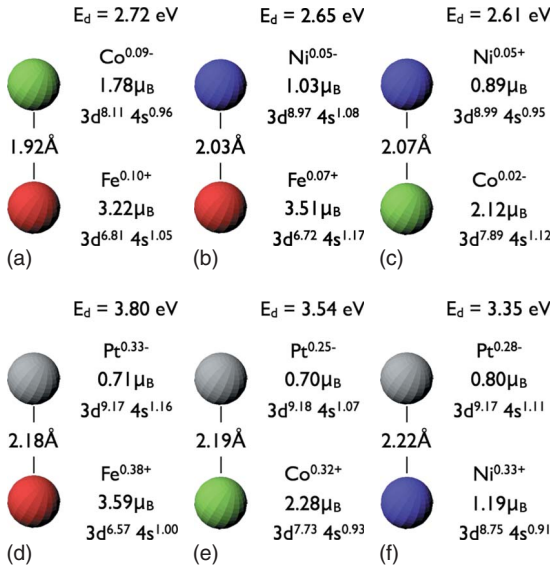

FIG. 9. (Color online) Dissociation energies (E_d), bond lengths, projected magnetic moments, and electronic configurations of the free FeCo, FeNi, CoNi, FePt, CoPt, and NiPt dimers. The color code for Fe, Co, Ni, and Pt is red, green, purple, and gray, respectively, and will be used throughout this paper. We note that the charges do not balance exactly and is a result of the errors introduced when calculating and integrating the projected density of states.

tain accurate magnetic moments for these dimers. Using zero smearing, we obtained a magnetic moment of $4.00\mu_B$ for both FeNi and FePt dimers. We found that the binding energy for the FeNi dimer as calculated using zero smearing is lower by 0.04 eV compared to the calculation where 0.001 Ry of smearing was used.

Six initial starting configurations for each of the FeCo, FeNi, CoNi, FePt, CoPt, and NiPt dimers adsorbed on graphene were studied. Representations of these configurations are shown in Fig. 6. For heteronuclear clusters there are two subconfigurations for each of 2.3 and 2.4 which we will refer to as configurations 2.n.1 and 2.n.2, where n=3 or 4, respectively. The former (latter) denotes the configuration where the atom with the lower (higher) atomic number is closer to the graphene. As the dimers do not have their bond axes oriented exactly perpendicular or parallel to the graphene plane, we define θ, which is the angle the dimer bond axis makes with the normal to the graphene plane. The angle θ is a useful measure of the extent of the buckling that occurs in the cases where the dimer bond axis is oriented nearly parallel to the graphene plane (i.e., in configurations 2.1 and 2.2). In the case of dimers adsorbed with the dimer bond axis oriented perpendicular to the graphene plane, we did not investigate the shape of the potential well associated with rotations about the normal to the surface. The optimized orientations for configurations 2.3.1, 2.3.2, 2.4.1, and 2.4.2

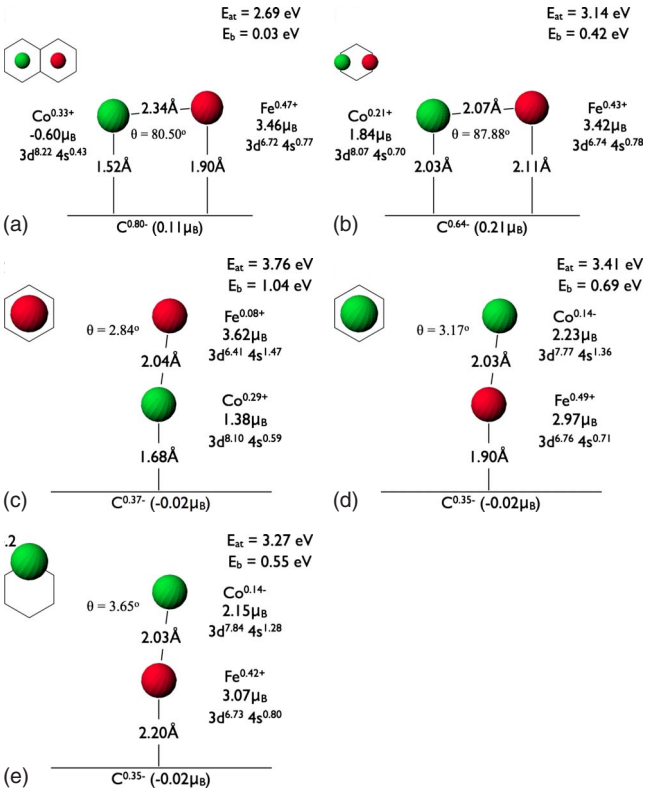

FIG. 10. (Color online) The atomization (E_{at}) and binding (E_b) energies, metal-metal bond lengths, metal-to-graphene separation, and projected magnetic moments and electronic configurations of the bound FeCo dimers. Configuration 2.4.1 is unstable and the dimer with that initial configuration converged to configuration 2.3.1.

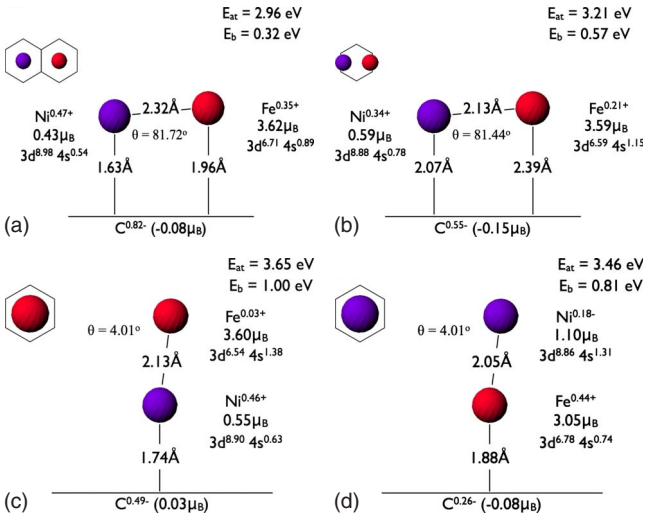

FIG. 11. (Color online) The atomization (E_{at}) and binding (E_b) energies, metal-metal bond lengths, metal-to-graphene separation, and projected magnetic moments and electronic configurations of the bound FeNi dimers. Configurations 2.4.1 and 2.4.2 are unstable and the dimers with those initial configurations converged to configurations 2.3.1 and 2.3.2, respectively

that we report here are found by starting with initial orientations that are exactly perpendicular to the graphene. At the optimized orientation, the resolved angular forces are smaller than 0.001 a.u. Although we did not do a comprehensive search for the minimum in the azimuthal direction, these small forces indicate that we are probably close to the bottom of a rotational well.

The most strongly bound FeCo, FeNi, and CoNi dimer configuration is 2.3.1. This corresponds to a dimer with its bond axis oriented nearly perpendicular to the graphene plane with the atoms directly above a hole site and the atom with the higher atomic number closer to graphene. The binding energies, the metal-metal bond lengths, the metal-to-graphene separation, and the projected magnetic moments and electronic configurations of the metal atoms for the bound FeCo, FeNi, and CoNi dimers are shown in Figs. 10–12. We added the binding energies to the respective free dimer bond energies to get atomization energies for the bound dimer. These values are also included in Figs. 10–12. As in the case of the homonuclear dimers, we also checked the convergence of the parameters used in our calculations by computing the atomization energies by taking the difference in the total energies of the graphene with two separate metal atoms in the gas phase and the graphene with the bound dimer. We find that the atomization energies calculated either way are the same.

The general trend electron population redistribution when the free heteronuclear dimer adsorbs on graphene is similar to that observed for homonuclear dimers. For example, the d-state occupancies for adsorbed heteronuclear dimers with bond axes nearly parallel to graphene are similar to those for the free dimer. Also, the s-state occupancy is considerably lower for the bound dimer compared to the free dimer; the depletion is again correlated with the amount of charge that is transferred to the π system of graphene. For the adsorbed

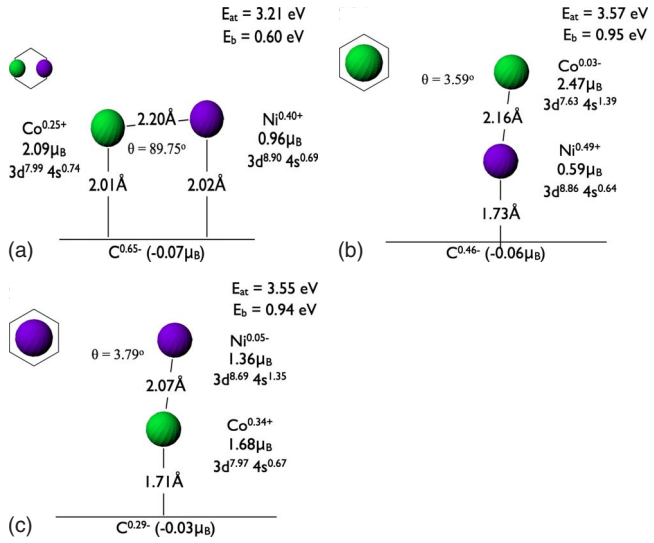

FIG. 12. (Color online) The atomization (E_{at}) and binding (E_b) energies, metal-metal bond lengths, metal-to-graphene separation, and projected magnetic moments and electronic configurations of the bound CoNi dimers. Configurations 2.1, 2.4.1, and 2.4.2 are unstable and the dimers with those initial configurations converged to configurations 2.2, 2.3.1, and 2.3.2, respectively

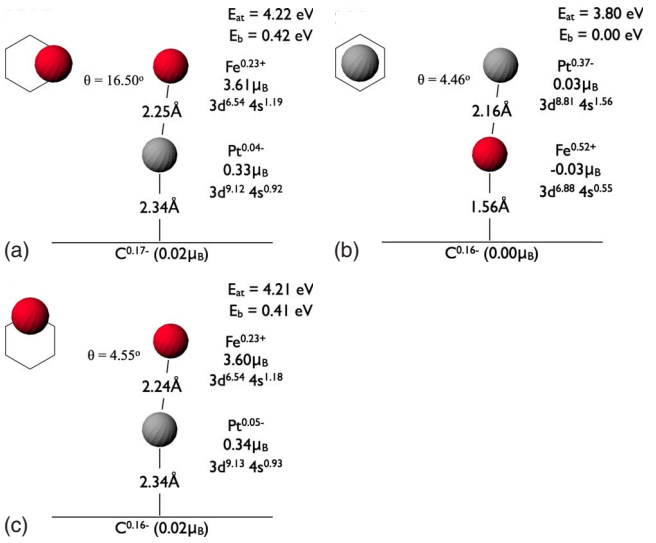

FIG. 13. (Color online) The atomization (E_{at}) and binding (E_b) energies, metal-metal bond lengths, metal-to-graphene separation, and projected magnetic moments and electronic configurations of the bound FePt dimers. Configuration 2.3.1 is unstable and the dimer with that initial starting configuration converged to the configuration labeled 2.3.1.0, with the Pt atom (closer to graphene) located above the bridge site (i.e., at the midpoint of the C-C bond in graphene). Configurations 2.1, 2.2, and 2.4.2 are unstable and the dimers with those initial configurations all converged to configuration 2.3.2, albeit the latter being the least stable of the bound FePt configurations studied in this work suggesting that the energy barrier to configuration 2.3.2 is lower than the energy barrier to configuration 2.3.1.0, the global minimum of the configurations studied here.

FeCo dimer in configuration 2.1, 0.80 electron is transferred to graphene. This is equal to the sum of the depletion in the *s*-state occupancies for the Fe and Co atoms, viz., 0.28 and 0.53, respectively. The projected electronic configuration for the atoms in a dimer bound with its axis nearly perpendicular to graphene is considerably different compared to a dimer bound with its axis nearly parallel to graphene. The atom that is farther from graphene has an electronic configuration that is closer to the free-atom electronic configuration. The *d*-state occupancy of the atom that is closer to graphene is similar to that of the projected electronic configuration in the free dimer. The charge transfer to the graphene comes almost entirely from the *s* orbital of the atom that is closer to graphene. For the bound FeCo dimer in configuration 2.3.1, the Co atom is closer to graphene. The change in the occupancy in the *s* state for this Co atom when the dimer goes from the free to bound state is equal to 0.37 [see Figs. 9 and 10(c)] and this is equal to the number of electrons transferred to the graphene. For dimers bound perpendicular to the graphene plane, desorption from the graphene is accompanied by a significant change in the electronic configuration of the atom farther from the graphene. For the bound FeCo dimer in configuration 2.3.1, the Fe atom electronic configuration changes from $3d^{6.41}4s^{1.47}$ to $3d^{6.81}4s^{1.05}$ when the dimer desorbs. Therefore desorption of perpendicular bound dimers is accompanied by an electronic interconfigurational energy change. This is not the case for dimers bound with their axes parallel to graphene and thus the perpendicularly bound dimers have a larger binding energy even though the amount of charge transferred to graphene is smaller. This also allows us to understand why configuration 2.3.2 has a lower binding energy than 2.3.1 because the interconfigurational $s \rightarrow d$ energy decreases as Fe > Co > Ni. This also explains why buckling occurs in dimer configurations 2.1 and 2.2 with the buckled-up atom having the higher interconfigurational $s \rightarrow d$ energy. The buckled-up atom has a slight depletion in its *d*-state occupancy and therefore a small amount of electron transfer to the *d* states is necessary in order to attain the electronic configuration of the free dimer. Having the buckled-up atom with the higher interconfigurational energy therefore allows for a small amount of added stability compared to a hypothetical case where both atoms have *d* occupancies that are very close to that of the free dimer. We also found that apart from the FeCo dimer bound as configuration 2.4.2, all other 2.4-type configurations were unstable. In these cases, the dimers migrated from the atom site to the hole site while maintaining the relative orientation of the dimer, viz., 2.4.1–2.3.1 and 2.4.2–2.3.2.

Just like the homonuclear dimers and the mixed FeCo, FeNi, and CoNi dimers, we find that the most strongly bound FePt, CoPt, and NiPt dimer configurations are those where the dimer bond axis is oriented nearly perpendicular to the graphene plane. The atomization and binding energies, metal-metal bond lengths, metal-to-graphene separation, and projected magnetic moments and electronic configurations of the metal atoms for the bound FePt, CoPt, and NiPt dimers are shown in Figs. 13–15, respectively, for dimer configurations which are stable. For these dimers, we were not able to find a stable configuration 2.1; the FePt and CoPt dimers with this initial configuration converged to configuration 2.3.2 while the NiPt dimer converged to configuration 2.2.

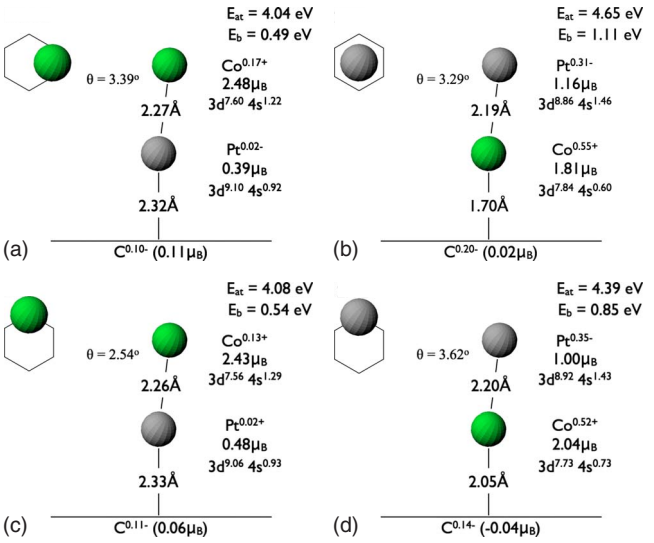

FIG. 14. (Color online) The atomization (E_{at}) and binding (E_b) energies, metal-metal bond lengths, metal-to-graphene separation, and projected magnetic moments and electronic configurations of the bound CoPt dimers. Like the FePt dimer bound with an initial configuration 2.3.1, the CoPt dimer converged to configuration 2.3.1.0. Configurations 2.1 and 2.2 are unstable and the dimers with those initial configurations both converged to configuration 2.3.2, which in the case of the bound CoPt, is the most stable of the bound CoPt dimer configurations studied in this work.

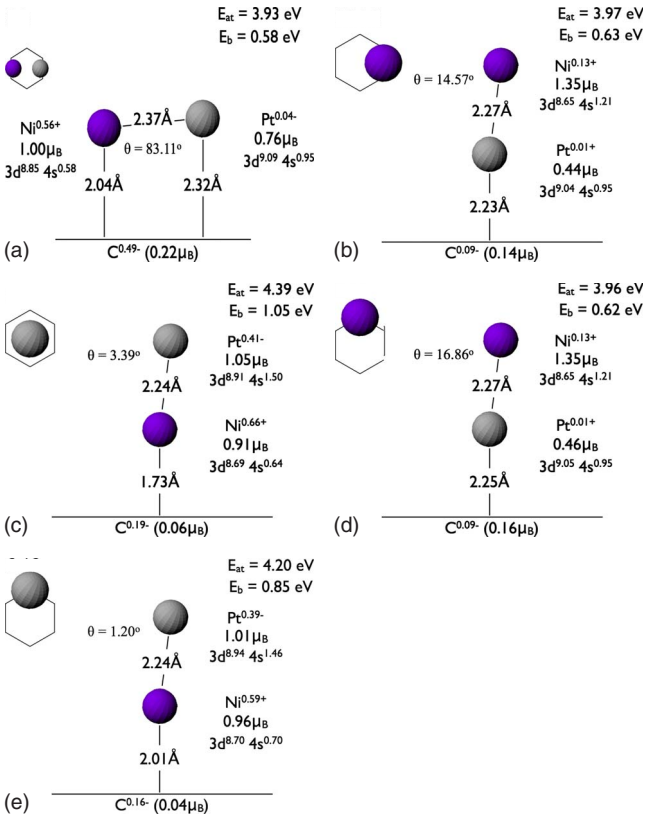

FIG. 15. (Color online) The atomization (E_{at}) and binding (E_b) energies, metal-metal bond lengths, metal-to-graphene separation, and projected magnetic moments and electronic configurations of the bound CoPt dimers. Like the FePt and CoPt dimers bound with an initial configuration 2.3.1, the NiPt dimer converged to configuration 2.3.1.0. Configuration 2.1 is unstable and the dimer with that initial configuration converged to configuration 2.2.

The most stable FePt configuration is 2.3.1.0 where the dimer is bound perpendicularly at a bridge site. The most stable CoPt and NiPt configuration is 2.3.2.

For the FePt, CoPt, and NiPt dimers, we find that configuration 2.3.1 is unstable. Starting with an initial configuration 2.3.1, these dimers migrated to the bridge site, which we have called configuration 2.3.1.0. We carried out calculations for Pt adatom on graphene and find that the bridge site is the most stable adsorption site. This has a binding energy of 1.44 eV and is 0.14 eV more stable than binding at an atom site. Our calculations showed that Pt atoms do not bind at the hole site. Given our previous discussion which demonstrates that electron transfer from perpendicularly bound dimers to graphene comes almost entirely from the atom closer to the graphene, the instability of the Pt adatom at the hole site is consistent with the instability of 2.3.1. This is further supported by the fact that configuration 2.1 is unstable for all three FePt, CoPt, and NiPt bound dimers, possibly owing to the fact that the Pt atom itself is unstable when bound above a hole site.

As opposed to the FeCo, FeNi, and CoNi dimers, the charge transfer that accompanies the adsorption of the FePt, CoPt, and NiPt dimers does not occur exclusively between the atom closer to graphene and graphene. The projected electronic configurations shown in Figs. 13–15 show that charge transfer also occurs between the two atoms of the dimer. However it is still clear that the atom farther from graphene has a larger electronic interconfigurational change, which in cases involves a net $d \rightarrow s$ interconfiguration change during adsorption. Since the $s \rightarrow d$ electronic interconfigurational energy for Pt is the most negative, we would expect that the X-Pt (X=Fe, Co, or Ni) dimers would adsorb most strongly with Pt closer to graphene. This is consistent for the adsorbed FePt dimer. However, the most strongly adsorbed CoPt and NiPt dimer configuration is one where the Pt atom is farther from graphene. As we have discussed earlier, the binding energy is determined by both the electronic interconfigurational energy change and the amount of charge transferred to the graphene. Our calculations suggest that for CoPt and NiPt, it is the effect of charge transfer that is dominant in determining the most stable adsorption configuration. For configurations where the Pt atom is closer to graphene, the lower charge transfer to graphene is consistent with the higher electronegativity of Pt relative to both Co and Ni. Thus, for CoPt and NiPt, the higher binding energies of configurations where the Pt atom is farther from graphene are ultimately due to the higher electronegativity of Pt.

Relative to the projected magnetic moments of the atoms in the free dimer, the projected magnetic moment of the atom that is farther from graphene is enhanced but is reduced for the atom that is closer to graphene. Overall, there is little change in the total magnetic moment of the dimer when bound to graphene compared to when it is free. To the best of our knowledge, there are no available data on the magnetic moment of the free FePt dimer but we would expect that since Pt is in the same group as Ni in the Periodic Table, the

total magnetic moment should be $4.00\mu_B$ as well; this is what we get in configurations 2.3.1.0 and 2.4.1. The total magnetic moment for FePt when bound as configuration 2.3.2 is zero. The spins on the two metal atoms are aligned antiferromagnetically and there is no net spin on graphene. For the free dimers, the projected moments on Fe, Co, and Ni are most enhanced when bonded to Pt and the projected magnetic moment on Pt is most enhanced when bonded to Ni. When the dimers are adsorbed on graphene, the projected moment on each of Fe, Ni, and Pt is most enhanced when bonded to Co in configurations 2.3.1, 2.3.2, and 2.3.2, respectively. For each combination of elements, these configurations are also the most stable ones found in our calculations except for the CoNi dimer for which configuration 2.3.1 is 0.01 eV more stable than configuration 2.3.2. The projected moment on Co is most enhanced when bonded to Fe in configuration 2.3.2 which has a binding energy that is 0.36 eV less than the most stable bound FeCo configuration, 2.3.1. Therefore, Fe, Ni, and Pt have their magnetic moments most enhanced when bonded to Co and bounded to graphene in the most stable dimer configuration or in a configuration that is very close in stability as in the case of the CoNi dimer.

IV. CONCLUSION

We have carried out plane-wave DFT calculations to investigate the binding, projected magnetic moments, and electronic configurations of Fe, Co, and Ni adatoms and dimers, both homonuclear and heteronuclear, the latter of which includes mixing with Pt, adsorbed on graphene. We found, contrary to previous work[6,7,50] that the Fe, Co, and Ni adatoms and homonuclear dimers bind weakly to graphene. The most stable adatom configuration corresponds to 1 where the atom is adsorbed above a hole site. The magnetic moment of the whole system (i.e., adatom and graphene) is $2\mu_B$ lower compared to the total magnetic moment of the unadsorbed atom and the plain graphene sheet. This is consistent with previous work.[6,7] For the homonuclear Fe, Co, and Ni dimers, there is little change in the total magnetic moments and dimer bond lengths compared to their free or unbound state. The most stable adsorbed homonuclear dimer configuration is configuration 2.3. This stability stems from the additional energy required for the electronic interconfiguration energy change in the atom farther from the graphene plane.

For each heteronuclear dimer we investigated, the most stable configurations are those where the dimer bond axis is oriented nearly perpendicular to the graphene plane. In these configurations (i.e., configurations of types 2.3 and 2.4), more energy is required to desorb the dimer relative to configurations where the dimer bond axis is oriented parallel to the graphene plane due to the additional energy required for an electronic interconfigurational change for the atom farther from the graphene. This is because this atom has an electronic configuration that is closer to that of the free atomic state rather than that of the free mixed dimer state. The most stable adsorbed FeCo, FeNi, and CoNi dimer configuration corresponds to 1 where the dimer bond axis is oriented nearly perpendicular to the graphene plane, with the atoms above a hole site and the species with the higher interconfiguration energy located farther from graphene. For the adsorbed FePt, CoPt, and NiPt dimers on graphene, we found that any hole site configuration is unstable and is most likely due to the fact that the Pt adatom is unstable above the hole site and migrates to the bridge site. We therefore found that configuration 2.3.1 is unstable and that a bound FePt, CoPt, and NiPt dimer with Pt closer to graphene converged to a structure where the dimer bond axis is perpendicular and above a bridge site (i.e., configuration 2.3.1.0). For the adsorbed FePt dimers on graphene, we found that the amount of charge transferred to graphene is the same regardless of the bound dimer configuration. The most stable FePt bound dimer configuration is 2.3.1.0, again where the metal atom, in this case Fe, with the higher interconfiguration energy is located farther from the graphene plane. For the CoPt and NiPt bound dimer configurations, we found that the charge transfer to the graphene plane is more significant than the interconfigurational change in determining the stability. The most stable adsorbed CoPt and NiPt dimers on graphene correspond to configuration 2.3.2, with the Co and Ni atoms, respectively, closer to graphene. The magnetic moment of the atom farther from (closer to) the graphene is enhanced (reduced) as in the case of the adsorbed homonuclear dimers. For the adsorbed mixed dimers, the magnetic moments of Fe, Ni, and Pt are most enhanced when bonded to Co. This enhancement of the magnetic moments of the Fe, Ni, and Pt atoms is largest for the most stable dimer configuration for each combination of elements.

Finally, since the accuracy of the interconfigurational energy is dependent on the level of approximation made for the exchange-correlation functional, we expect improvements in the exchange-correlation functional to lead to better estimates of the binding energy.

*chmkhc@nus.edu.sg

[1] C. Köhler, G. Seifert, and T. Frauenheim, Chem. Phys. **309**, 23 (2005).
[2] C. Jamorski, A. Martinez, M. Castro, and D. R. Salahub, Phys. Rev. B **55**, 10905 (1997).
[3] M. Castro, C. Jamorski, and D. R. Salahub, Chem. Phys. Lett. **271**, 133 (1997).
[4] M. C. Michelini, R. P. Diez, and A. H. Jubert, Int. J. Quantum Chem. **70**, 693 (1998).
[5] M. C. Michelini, R. P. Diez, and A. H. Jubert, Int. J. Quantum Chem. **85**, 22 (2001).
[6] Y. Yagi, T. M. Briere, M. H. F. Sluiter, V. Kumar, A. A. Farajian, and Y. Kawazoe, Phys. Rev. B **69**, 075414 (2004).
[7] D. M. Duffy and J. A. Blackman, Phys. Rev. B **58**, 7443 (1998).
[8] Y. Xie and J. A. Blackman, Phys. Rev. B **66**, 085410 (2002).
[9] A. Bergman, E. Holmström, A. M. N. Niklasson, L. Nordström,

S. Frota-Pessôa, and O. Eriksson, Phys. Rev. B **70**, 174446 (2004).
[10] G. Mpourmpakis, G. E. Froudakis, A. N. Andriotis, and M. Menon, Phys. Rev. B **72**, 104417 (2005).
[11] V. S. Stepanyuk, W. Hergert, K. Wildberger, R. Zeller, and P. H. Dederichs, Phys. Rev. B **53**, 2121 (1996).
[12] B. Lazarovits, L. Szunyogh, and P. Weinberger, Phys. Rev. B **65**, 104441 (2002).
[13] X. Du, M. Inokuchi, and N. Toshima, J. Magn. Magn. Mater. **299**, 21 (2006).
[14] C. Petit, S. Rusponi, and H. Brune, J. Appl. Phys. **95**, 4251 (2004).
[15] C. Chinnasamy, B. Jeyadevan, K. Shinoda, and K. Tohji, J. Appl. Phys. **93**, 7583 (2003).
[16] C. Antoniak *et al.*, Phys. Rev. Lett. **97**, 117201 (2006).
[17] K. T. Chan, J. B. Neaton, and M. L. Cohen, Phys. Rev. B **77**, 235430 (2008).
[18] M. Castro and D. R. Salahub, Phys. Rev. B **49**, 11842 (1994).
[19] B. N. Papas and H. F. Schaefer III, J. Chem. Phys. **123**, 074321 (2005).
[20] M. Menon, A. N. Andriotis, and G. E. Froudakis, Chem. Phys. Lett. **320**, 425 (2000).
[21] H.-J. Fan, C.-W. Liu, and M.-S. Liao, Chem. Phys. Lett. **273**, 353 (1997).
[22] A. N. Andriotis, G. Mpourmpakis, G. E. Froudakis, and M. Menon, J. Chem. Phys. **120**, 11901 (2004).
[23] S. S. Peng, B. R. Cooper, and Y. G. Hao, Philos. Mag. B **73**, 611 (1996).
[24] M. Bäumer, J. Libuda, and H. J. Freund, Surf. Sci. **327**, 321 (1995).
[25] P. Krüger, A. Rakotomahevitra, J. C. Parlebas, and C. Demangeat, Phys. Rev. B **57**, 5276 (1998).
[26] A. N. Andriotis, M. Menon, and G. E. Froudakis, Phys. Rev. B **62**, 9867 (2000).
[27] A. N. Andriotis and M. Menon, Phys. Rev. B **60**, 4521 (1999).
[28] A. K. Geim and K. S. Novoselov, Nature Mater. **6**, 183 (2007).
[29] T. Ohta, A. Bostwick, T. Seyller, K. Horn, and E. Rotenberg, Science **313**, 951 (2006).
[30] K. S. Novoselov, E. McCann, S. V. Morozov, V. I. Fal'ko, M. I. Katsnelson, U. Zeitler, D. Jiang, F. Schedin, and A. K. Geim, Nat. Phys. **2**, 177 (2006).
[31] G. Li and E. Y. Andrei, Nat. Phys. **3**, 623 (2007).
[32] B. Uchoa and A. H. Castro Neto, Phys. Rev. Lett. **98**, 146801 (2007).
[33] S. Y. Zhou, G. D. Gweon, J. Graf, A. V. Fedorov, C. D. Spataru, R. D. Diehl, Y. Kopelvich, D. D. Lee, S. G. Louie, and A. Lanzara, Nat. Phys. **2**, 595 (2006).
[34] S. W. Poon, J. S. Pan, and E. S. Tok, Phys. Chem. Chem. Phys. **8**, 3326 (2006).
[35] S. H. Vosko, L. Wilk, and M. Nusair, Can. J. Phys. **58**, 1200 (1980).
[36] J. P. Perdew and Y. Wang, Phys. Rev. B **45**, 13244 (1992).
[37] S. Baroni, A. D. Corso, S. de Gironcoli, and P. Giannozzi, PWSCF, 2008 (http://www.pwscf.org).
[38] A. M. Rappe, K. M. Rabe, E. Kaxiras, and J. D. Joannopoulos, Phys. Rev. B **41**, 1227 (1990).
[39] J. P. Perdew, K. Burke, and M. Ernzerhof, Phys. Rev. Lett. **77**, 3865 (1996).
[40] S. Baroni, A. D. Corso, S. de Gironcoli, and P. Giannozzi, PWSCF pseudopotentials, 2008 (http://www.pwscf.org/pseudo.htm).
[41] N. Marzari, D. Vanderbilt, A. De Vita, and M. C. Payne, Phys. Rev. Lett. **82**, 3296 (1999).
[42] J. Izquierdo, A. Vega, L. C. Balbás, D. Sánchez-Portal, J. Junquera, E. Artacho, J. M. Soler, and P. Ordejón, Phys. Rev. B **61**, 13639 (2000).
[43] S. Yanagisawa, T. Tsuneda, and K. Hirao, J. Chem. Phys. **112**, 545 (2000).
[44] E. G. Moroni, G. Kresse, J. Hafner, and J. Furthmüller, Phys. Rev. B **56**, 15629 (1997).
[45] J. Harris and R. O. Jones, J. Chem. Phys. **70**, 830 (1979).
[46] H.-T. Jeng and C.-S. Hsue, Phys. Rev. B **62**, 9876 (2000).
[47] F. W. Kutzler and G. S. Painter, Phys. Rev. B **43**, 6865 (1991).
[48] N. Marzari and Y. S. Lee, Convergence tests for c.pbe-rrkjus.upf—total energy of graphite $6\times6\times4$ *k*-point grid: *ecutwfc*=24, 26, 28, 30, and 32; *ecutrho*=160, 200, and 240, 2008 (http://www.pwscf.org/pseudo/1.3/UPF/C.pbe-rrkjus-test-graphite.pdf).
[49] H. J. Monkhorst and J. D. Pack, Phys. Rev. B **13**, 5188 (1976).
[50] Y. Mao, J. Yuan, and J. Zhong, J. Phys.: Condens. Matter **20**, 115209 (2008).
[51] E. J. Duplock, M. Scheffler, and P. J. D. Lindan, Phys. Rev. Lett. **92**, 225502 (2004).
[52] T. Noro, C. Ballard, M. H. Palmer, and H. Tatewaki, J. Chem. Phys. **100**, 452 (1994).
[53] E. A. Rohlfing, D. M. Cox, A. Kaldor, and K. H. Johnson, J. Chem. Phys. **81**, 3846 (1984).
[54] M. Moskovits, D. P. DiLella, and W. Limm, J. Chem. Phys. **80**, 626 (1984).
[55] L. Lian, C.-X. Su, and P. B. Armentrout, J. Chem. Phys. **97**, 4072 (1992).
[56] D. A. Hales, C.-X. Su, L. Lian, and P. B. Armentrout, J. Chem. Phys. **100**, 1049 (1994).
[57] L. M. Russon, S. A. Heidecke, M. K. Birke, J. Conceicao, M. D. Morse, and P. B. Armentrout, J. Chem. Phys. **100**, 4747 (1994).
[58] M. D. Morse, G. P. Hansen, P. R. R. Langridge-Smith, L.-S. Zheng, M. E. Geusic, D. L. Michalopoulos, and R. E. Smalley, J. Chem. Phys. **80**, 5400 (1984).
[59] A. Kokalj, Comput. Mater. Sci. **28**, 155 (2003).
[60] S. Yanagisawa, T. Tsuneda, and K. Hirao, J. Comput. Chem. **22**, 1995 (2001).